REPUBLIC OF TURKEY
ISTANBUL GELISIM UNIVERSITY
INSTITUTE OF GRADUATE STUDIES

Department of Electrical and Electronics Engineering

DESIGNING AN EFFECTIVE MIMO ANTENNA FOR 5G

Master Thesis

Dunya Jasim Albu MOHAMMED

Supervisor

Asst. Prof. Dr. A. F. M. Shahen SHAH

Istanbul – 2023

THESIS INTRODUCTION FORM

Name and Surname	: Dunya Jasim Albu Mohammed
Language of the Thesis	: English
Name of the Thesis	: Designing An Effective MIMO Antenna for 5G
Institute	: Istanbul Gelisim University Institute of Graduate Studies
Department	: Electrical and Electronics Engineering
Thesis Type	: Master
Date of the Thesis	: 26/12/2022
Page Number	: 85
Thesis Supervisors	: Asst. Prof. Dr. A. F. M. Shahen Shah
Index Terms	: Ultra-wide band (UWB) antennas, 5G, Millimeter wave (mm-Wave), MIMO, wireless communication.

Turkish Abstract : Kablosuz iletişim sistemlerinin geliştirilmesinde etkin bir anten tasarımı oldukça önemlidir. Bu çalışmada, 5G mobil ağlar gibi ultra geniş bant uygulamalarında kullanılmak üzere altıgen bir mikroşerit antenin tasarımı ve modellenmesi sunulmaktadır. Önerilen anten, 3.3 GHz ila 4.5 GHz frekans aralığına, 20 mm × 14 mm boyutlara sahiptir ve 4.3 bağıl geçirgenliğe ve 1.6 mm yüksekliğe sahip bir FR-4 alt tabaka üzerine inşa edilmiştir. Bu antenin 3.3 GHz ve 4.5 GHz rezonans frekansları ve 2'den küçük bir voltaj duran dalga oranı (voltage standing wave ratio, VSWR) ile iki dişli bantta çalışması beklenmektedir. Çoklu giriş çoklu çıkış (multiple input multiple output, MIMO) anteni olacak şekilde genişletilen önerilen anten,

CST Microwave Studio kullanılarak oluşturulmuş ve modellenmiştir.

Distribution List : 1. To the Institute of Graduate Studies of Istanbul Gelisim University
2. To the National Thesis Center of YÖK (Higher Education Council)

Dunya Jasim Albu Mohammed

REPUBLIC OF TURKEY
ISTANBUL GELISIM UNIVERSITY
INSTITUTE OF GRADUATE STUDIES

Department of Electrical and Electronics Engineering

DESIGNING AN EFFECTIVE MIMO ANTENNA FOR 5G

Master Thesis

Dunya Jasim Albu MOHAMMED

Supervisor

Asst. Prof. Dr. A. F. M. Shahen SHAH

Istanbul – 2023

DECLARATION

I hereby declare that in the preparation of this thesis, scientific ethical rules have been followed, the works of other persons have been referenced in accordance with the scientific norms if used, there is no falsification in the used data, any part of the thesis has not been submitted to this university or any other university as another thesis.

Dunya Jasim Albu Mohammed

…/…/2023

TO ISTANBUL GELISIM UNIVERSITY

THE DIRECTORATE OF GRADUATE EDUCATION INSTITUTE

The thesis study of Dunya Jasim Mohammed ALBU MOHAMMED titled as ''Designing An Effective MIMO Antenna for 5G'' has been accepted as MASTER in the department of Electrical and Electronics Engineering by the jury.

Director

Asst. Prof. Dr. A.F.M. Shahen SHAH

(Supervisor)

Member

Assoc. Prof. Dr. Indrit MYDERRIZI

Member

Asst. Prof. Dr. A.F.M. Suaib AKHTER

APPROVAL

I approve that the signatures above signatures belong to the aforementioned faculty members.

... / ... / 20..

Prof. Dr. Izzet GUMUS

Director of the Institute

SUMMARY

In the development of wireless communication systems, an effective antenna design is crucial. In this work, the design and modeling of a hexagonal microstrip antenna is presented for use in ultra-wide band applications such as 5G mobile networks. The suggested antenna has a frequency range of 3.3 GHz to 4.5 GHz, dimensions of 20 mm × 14 mm, and is built on a FR-4 substrate, with a relative permittivity of 4.3, and of 1.6 mm in height. It is expected that this antenna will operate in two notched bands with resonance frequencies of 3.3 GHz and 4.5 GHz and a voltage standing wave ratio (VSWR) of less than 2. The proposed antenna, which has been expanded to be a multiple-input multiple-output (MIMO) antenna, was created and modeled using CST Microwave Studio.

Keywords: Antenna, MIMO, wireless communication, 5G, Ultra-Wide Band (UWB) antennas, Millimeter wave (mm-Wave).

ÖZET

Kablosuz iletişim sistemlerinin geliştirilmesinde etkin bir anten tasarımı oldukça önemlidir. Bu çalışmada, 5G mobil ağlar gibi ultra geniş bant uygulamalarında kullanılmak üzere altıgen bir mikroşerit antenin tasarımı ve modellenmesi sunulmaktadır. Önerilen anten, 3.3 GHz ila 4.5 GHz frekans aralığına, 20 mm × 14 mm boyutlara sahiptir ve 4.3 bağıl geçirgenliğe ve 1.6 mm yüksekliğe sahip bir FR-4 alt tabaka üzerine inşa edilmiştir. Bu antenin 3.3 GHz ve 4.5 GHz rezonans frekansları ve 2'den küçük bir voltaj duran dalga oranı (voltage standing wave ratio, VSWR) ile iki dişli bantta çalışması beklenmektedir. Çoklu giriş çoklu çıkış (multiple input multiple output, MIMO) anteni olacak şekilde genişletilen önerilen anten, CST Microwave Studio kullanılarak oluşturulmuş ve modellenmiştir.

Anahtar Kelimeler: Anten, MIMO, kablosuz haberleşme, 5G, Milimetre dalga (mm-Dalga), Federal İletişim Komisyonu (FCC) yetki veriyor.

TABLE OF CONTENTS

CHAPTER ONE

INTRODUCTİON AND LITERATURE SURVEY

CHAPTER TWO

CIRCULAR MIMO ANTENNA OPERATING IN 5G

CHAPTER THREE

SINGLE HEXAGON ANTENNA

CHAPTER FOUR

PROPOSED MIMO HEXAGON ANTENNA

CHAPTER FIVE

CONCLUSIONS AND SUGGESTIONS FOR FUTURE WORKS

ABBREVIATIONS

Abbreviation	Meaning
4G	Fourth- generation
5G	Fifth- generation
BW	Bandwidth
CST	Computer Simulation Technology
FCC	Federal Communications Commission
FR4	Flame Resistant 4
GHz	Gigahertz
GPS	Global Positioning System
GSM	Global System for Mobile Communications
HDR	high-data-rate
HLAN	Hyper Local Area Network
IEEE	Institute of Electrical and Electronics Engineers
IMT	International Mobile Telecommunications
MIMO	multiple-input and multiple-output
UWB	ultra-wideband
LDR	low-data-rate
VSWR	voltage standing wave ratio

LIST OF TABLES

LIST OF FIGURES

PREFACE

At first, I express my heartiest thanks and gratefulness to almighty ALLAH for HIS divine blessings, which made me possible to complete the thesis successfully in time. I would like to thank my Master advisor Asst. Prof. Dr. A. F. M. Shahen Shah. This thesis would not have been possible without his extensive background and interest in the topic, his boundless patience and encouragement, his constant and energetic supervision, his constructive criticism and advice, and his diligence in reading numerous subpar drafts and making necessary corrections. I'll always be grateful to him for believing in me and giving me plenty of chances to grow as a researcher. I'd like to thank the thesis jury members Assoc. Prof. Dr. Indrit MYDERRIZI and Asst. Prof. Dr. A.F.M. Suaib AKHTER for their assistance in managing and moving this thesis ahead with their insightful remarks and ideas throughout the process.

Finally, I'd want to thank my family for their support.

CHAPTER ONE

INTRODUCTION AND LITERATURE SURVEY

1.1 Introduction

Wireless communication via electromagnetic waves has grown in popularity over the last decade. The antenna is one of the most critical components of any wireless communications system that works on the transmitter or receiver side of the wireless device (Azari & propagation, 2011). The antennas have various types, sizes, shapes, and functionality; each has its own set of characteristics and applications. There are several kinds, including monopole/dipole, reflector, slot antenna, patch antenna, a folded dipole antenna, and microstrip antenna (Balanis, 2015).

With the coming of the Internet of Things (IoT) and realistic Ultra High Definition (UHD) services, it is expected to multiply mobile traffic due to increasing mobile devices. This stunning rise necessitates a significant increase in mobile network capacity beyond today's 3G/4G networks to the next generation of wireless radio standards (Kabalci & Kabalci, 2019).

Therefore, the 5th Generation (5G) has been introduced as an integrative system that integrates the currently implemented wireless networking systems, such as Long Team Evaluation (LTE) and Wireless Fidelity (Wi-Fi), into a single air interface, thus increasing response time, energy efficiency, and network reliability (Al-Ogaili & Shubair, 2016). High frequencies are associated with short wavelengths ranging from 1 to 10 mm for millimeter- waves (mm-waves) (Al-Ani, Al-Ani, Mosleh, & Abd-Alhameed, 2021). The mm-wave cellular systems appear to be a promising nominee for next-generation cellular systems, which are expected to accommodate data speeds of several gigabits per second. However, the use of mm-wave necessitates consideration of propagation characteristics and channel deterioration of the high-frequency bands (Yassein, Aljawarneh, & Al-Sadi, 2017).

The main impediments to mm-wave propagation are higher path loss because of reduced scattering, which decreases the available diversity, higher carrier frequency, and increased effect of blockage due to weaker non-line-of-sight paths. Accordingly, the noise power effect is more pronounced because of the larger bandwidth usage (Ahad et al., 2020). Multiple-Input Multiple-Output (MIMO) antenna systems compensate for

high attenuation and dispersal of 5G band frequencies (Talwar et al., 2014). However, Massive MIMO (MA-MIMO) refers to a MIMO device that consists of many antennas with dynamic directivity capability and prefers diversity to boost mm-wave efficiency. MA-MIMO is thought to be a primary enabler for 5G communication systems (Zerihun & Wondie, 2017). For a MIMO system to operate competently, there should be very low Mutual Coupling (MC) between the ports. Placing the antenna elements at a minimum distance of λ/2 decreases MC. Still, since mobile devices are so small these days, antenna elements must be located very close to each other, which increases coupling (Irene & Rajesh, 2018). The MIMO antenna using polarization diversity addresses this problem of MC (Talwar et al., 2014).

There are three significant types of polarization: Linear Polarization (LP), Circular Polarization (CP), and Elliptical Polarization (EP). Also, it can be considered that the LP and the CP are a particular case of EP (Khoshniat, 2011). However, compared to LP radiators, CP antenna elements have many important advantages in terms of radio wave propagation. CP antennas, for example, efficiently mitigate the effects of multipath fading and are therefore resistant to polarization mismatch. Furthermore, regardless of the CP antenna orientation, the force of the Electromagnetic (EM) signals obtained at the wireless terminals is relatively constant. Due to these characteristics, CP antennas are possible candidates for future MIMO wireless systems (Saxena et al., 2020). Accordingly, it seems that the characteristics of CP antennas make them a better choice for future MIMO wireless systems to achieve low mutual coupling. The motivation of this thesis is to approach an optimum design of a MIMO antenna based on CP that will offer good performance, high isolation with low complexity, and a compact size.

1.2 MIMO Technology

The MIMO is a technology that uses numerous transceivers to transfer more data at once and is used in mobile phone networks. This technique aims to improve system capacity without utilizing extra bandwidth, where capacity is directly proportional to the number of antennas on the transceiver. It provides a larger data rate at a lower cost, but it may add to the system's complexity (Tsoulos, 2018). Figure 1.1 depicts a MIMO system.
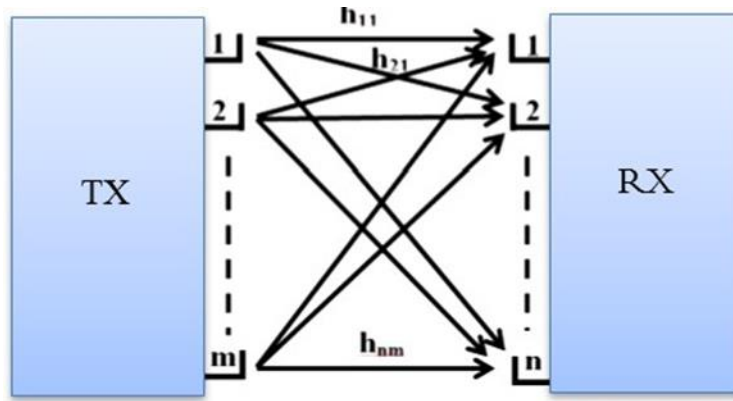
Figure 1. 1 MIMO system (Agboje et al., 2020)

MIMO systems can employ two distinct transmission techniques, which are (Kiani et al., 2020):

1.2.1 Space Time Coding (STC)

A technique is used to enhance data transmission reliability using multiple transmit antennas in wireless communication systems. STC sends multiple redundant data stream copies to the receiver, so at least one of them survives through the channel between transmitter and receiver to allow reliable decoding. Accordingly, the MIMO system performance is enhanced by achieving a diversity gain as shown in figure 1.2.
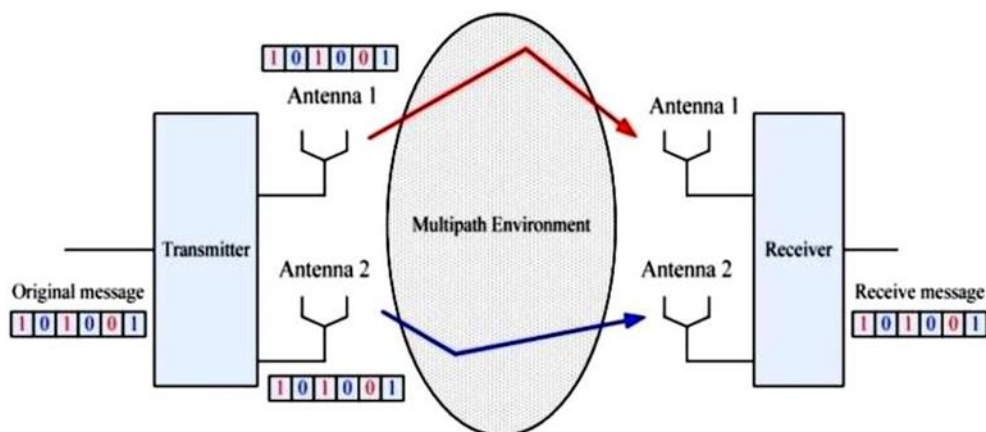
Figure 1. 2 The structure of STC (Kiani et al., 2020)

3

1.2.2 Space Division Multiplexing (SDM)

To improve system capacity, it has been used Space Division Multiplexing (SDM), which is a promising technology where every MIMO system antenna transmits different data streams simultaneously and in parallel channels. As shown in figure 1.3, the transmitted data is split into sub-data streams that are transmitted by different antennas at the same time. Then the streams are mixed together to regenerate the original data stream at the receiving antennas.
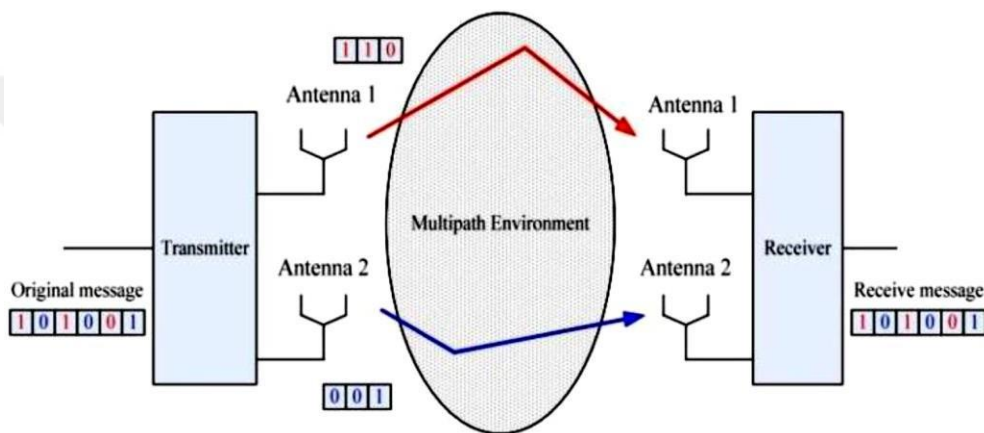
Figure 1. 3 The structure of SDM (Kiani et al., 2020)

Each MIMO system could contain a mixture of STC and SDM to have the ability to achieve communication system reliability and/or better channel capacity (Kiani et al., 2020).

In addition to what was mentioned above, MIMO is considered one of the leading enabling technologies for 5G mobile communication networks, which was launched in early 2020. Its target is to improve the network capacity by providing high data rates and multimedia for inflow for users. It used mm-waves, which operate in the 24-300 GHz band, which are the high frequencies concerned with short wavelengths. However, mm-waves can be absorbed easily by nearby buildings, trees, raindrops, and gases in the air. As a result, the impairment factors are the critical challenges in the mm-waves spectrum. So, the combination of 5G technology with the MIMO system is the ideal solution to the above problem, compensating for a lot of attenuation facing the 5G frequency band.

1.3 Literature Survey

In 2017 (Xu et al., 2017), Xu, Rui, et al. Proposed a compact size CP antenna for triple-wideband feeding by microstrip-line. It contains an L-shaped radiator pattern at the top layer and two rectangular strips at the ground structure for wider Axial Ratio Bandwidths (ARBWs) and the widest Impedance Bandwidths (IBWs).

In 2018 (Mathur, Dwari, & Communications, 2018), Mathur, Rohit, et al. Proposed a Coplanar Waveguide (CPW) fed MIMO antenna to operate in the Ultra-Wideband (UWB) frequency range of 3-12 GHz with high fractional bandwidth of 120% to keep isolation better than 15 dB.

In 2018 (Xiong, Ling, Zhang, Zhang, & applications, 2018), Xiong, Xuan, et al. Present a CPW-fed MIMO antenna for CP with multi-bandwidth and higher isolation. The CP frequency range includes the LTE (from1.71 to 2.17 GHz), the WCDMA (from1.92 to 2.17 GHz), the WLAN (from 2.3 to 2.5 GHz), and the WiMax (from 2.3 to 2.5 GHz).

In 2018 (Shoaib et al., 2018), Shoaib, Nosherwan, et al. The proposed compact MIMO system comprises eight antenna elements for future 5G devices, with a size of 3×4 mm2. The ground plane is a structure based on electromagnetic bandgaps designed to improve gain and efficiency.

In 2019 (Parchin et al., 2019), Parchin, Naser Ojaroudi, et al. Presented an eight-port dual-polarized MIMO antenna for 5G applications. The proposed antennas are designed to operate at 3.6 GHz and are arranged on the smartphone Printed Circuit Board (PCB) corners to offer full radiation coverage with various polarizations.

In 2019 (Subhanrao Bhadade & Padmakar Mahajan, 2019), Subhanrao, Raghunath, et al. Proposed a CP four- element MIMO antenna with high isolation to operate at a resonant frequency in the 2.4 GHz WLAN band. The MIMO design is dependent on orthogonal geometry to decrease the mutual coupling between the elements.

In 2019 (Chakraborty et al., 2019), Chakraborty, Swarup, et al. Proposed a two-element MIMO antenna with CP diversity to operate in sub-6 GHz with an operation band (3.6-3.8 GHz) for 5G wireless applications. That achieved a good isolation loss of -25 dB among antenna elements and an Axial Ratio (AR) of less than 0.5 dB.

In 2019 (Iqbal et al., 2019), Iqbal, Javed, et al. Presented a novel wideband two-elements CP-MIMO Dielectric Resonator Antenna (DRA) for WiMAX applications, with a wide bandwidth of 38.51% (3.50–4.95 GHz), low mutual coupling <-28 dB, and broadband CP of 20.82% (3.58–4.40 GHz).

In 2019 (Midya, Bhattacharjee, Mitra, & Letters, 2019), Midya, Manas, et al. Design a compact CP monopole antenna with an overall size of 30×32 mm2. Two orthogonal modes with identical amplitude and 900 Phase Difference (PD) for CP are formed by protruding a G-shaped parasitic strip into a C-shaped monopole antenna construction (CP).

In 2020 (Kumar, Urooj, & Alrowais, 2020), Kumar, Pawan, et al. Proposed a four-element MIMO antenna for dual-band notched property Wi-MAX (3.5 GHz) and WLAN (5.5 GHz) that was achieved by inserting a Hexagonal-Shaped Complementary Split-Ring Resonator (HCSRR) for UWB application.

In 2020 (S. Kumar et al., 2020), Kumar, Sachin, et al. Present a four-port UWB-MIMO diversity antenna with dual-band elimination property. The orthogonally schematic is used to arrange the four similar rhombic-shaped monopole radiators to improve isolation between ports and polarization diversity.

In 2020 (Ojaroudi Parchin, Jahanbakhsh Basherlou, IA Al-Yasir, M. Abdulkhaleq, & A. Abd-Alhameed, 2020), Ojaroudi Parchin, Naser, et al. Proposed a four-element UWB-MIMO antenna of 75×150 mm2 for future smartphones. It is based on a dual-polarized port. Each dual antenna consists of a circular-ring slot radiator with an open-end fed by two semi-arc-shaped microstrip feeding lines that offer polarization diversity.

In 2020 (Chakraborty et al., 2020), Chakraborty, Swarup, et al. Presented a four-element MIMO antenna with orthogonal CP aiming to use the antenna system in sub-6 GHz 5G applications, which provides CP gain and good isolation in the full band (3.4–3.8 GHz).

In 2020 (Hussain, Jeong, Abbas, & Kim, 2020), Hussain, Niamat, et al. Presented a metasurface (MS) based CP-MIMO system with the wideband operation. The antenna's

operational bandwidth spans the mm-wave band (25–29.5 GHz), which is designated for 5G communication.

1.4 Thesis Objectives

a.   The methodology of this thesis starts with a single antenna element with hexagon design. After evaluating this antenna element, they integrated four replicas onto the PCB corners to investigate both the single-element matching results as well as the performance of such a MIMO antenna system.

b.   Present a variety of MIMO antenna system designs that operate frequent frequency bands to meet future communication requirements.

c.   To compare the performance of the proposed design to other previous work in this field, in addition to trying to improve the performance in terms of the operating bandwidth and correlation coefficient.

1.5 Thesis Outlines

This thesis is divided into five chapters, which are listed below:

Chapter 1: contains an overview of the thesis, Literature Survey, Thesis Objectives, and Thesis Outline details.

Chapter 2: includes the fifth mobile generation concept in terms of the candidate frequency bands and merges this technology with the MIMO system. Also, the definition of antenna polarization and its types. In addition to a deep explanation of CP antennas and their benefits.

Chapter 3: Presents designs of single antenna design. The antenna elements were printed on the PCB in two ways, symmetrical and orthogonal, to obtain the best results in terms of mutual coupling and bandwidth.

Chapter 4: The proposed MIMO antenna performance results are presented, such as S- parameter, Voltage Standing Wave Ratio (VSWR), radiation pattern for single antenna elements, and some results from evaluating step antennas. In addition, some parameters of the MIMO system to evaluate its performance, such as MC, Envelop

Correlation Coefficient (ECC), Diversity Gain (DG), Mean Effective Gain (MEG), and Channel Capacity Loss (CCL) will be presented.

Chapter 5: Includes conclusions are drawn from the works presented in this thesis, and some suggestions.

CHAPTER TWO

CIRCULAR MIMO ANTENNA OPERATING IN 5G

2.1 Introduction

Nowadays, the fast developments in applications of wireless push many RF devices to work with multimode operations and different communication standards to support various services. Multiple service standards can be translated into multiband antennas or multiple antennas used in one device from a practical perspective. This chapter presents the services and applications of 5G, candidate frequency bands for the 5G system, the methods to address the mutual coupling problem facing MIMO antennas for 5G, antenna polarization type, and CP with feed techniques and their benefits.

2.2 Fifth Mobile Generation (5G)

Mobile communication is one of the most exciting fields of advanced technology. These technologies have passed through several generations or stages of enhancement and evolution in their performance. The First Generation (1G) was referred to as cellular, then abbreviated to "cell" later. In nature, cell phone signals are analog. The 1G device was comparatively expensive and less heavy. While in the second generation (2G), users can rely on a digital signal for the first time. These emerging technology-enabled users benefit from Short Message Services (SMS) and more voice capacity. The Third Generation (3G) allowed mobile telephone users to use graphics, voice, and video applications. Then, the fourth generation (4G), also known as LTE, was developed in 2010, used for handheld devices and cell phones. It can transfer data up to 10 times faster than 3G (A. S. D. Shah, 2022).

By 2020, the 5th Generation (5G) was introduced, whose development depends upon 4G. At present, it is struggling to meet its performance goals. This generation will connect mobile terminals (users) and everything surrounding those users (Internet of Things) with excellent features such as no latency, high data rates (up to 10Gbps), and robust communications independent of geographical position (Chataut & Akl, 2020; Gupta & Technology, 2015). The evolution of mobile communication from 1G to 5G is shown in figure 2.1.
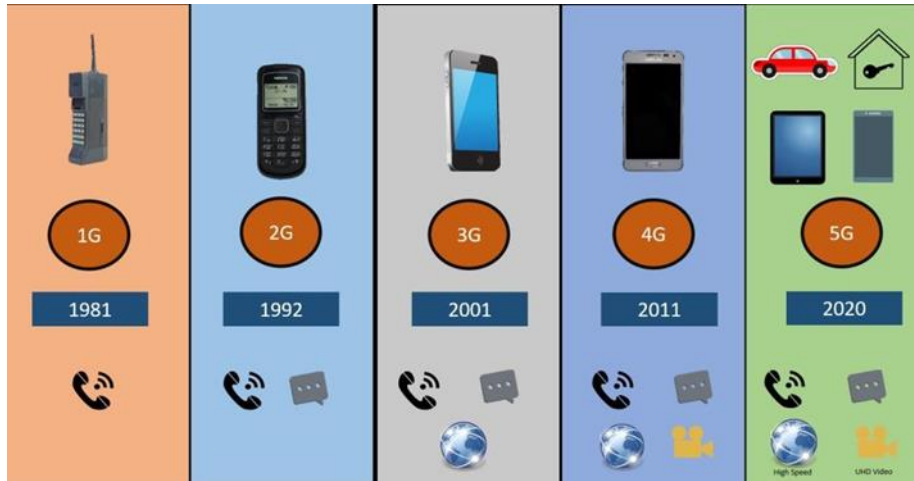
Figure 2. 1 The evolution of mobile communication (Chataut & Akl, 2020).

5G mobile technologies should support and provide many applications and services, according to the UK's communication regulator (Ofcom). These services need different coverage, speed, and reliability requirements, so those different deployment models, spectrum bands, and network solutions are highly required. These applications and services can be divided into three groups (Ofcom, 8 February 2017), as shown in figure 2.2.

Figure 2. 2 5G applications sketch (Ofcom, 8 February 2017)

a. Mobile Broadband Enhancement, With the evolution of 4G's already- existing services, 5G is predicted to provide more reliable and faster mobile broadband, offering a wealthier experience to consumers (Shah, 2022).

b. 5G should help the IoT applications and services evolution and enhance interaction between various platforms. Future applications could include street lighting optimization to suit the traffic or weather, patients' real-time health monitoring, smart agriculture, and environmental monitoring. Data privacy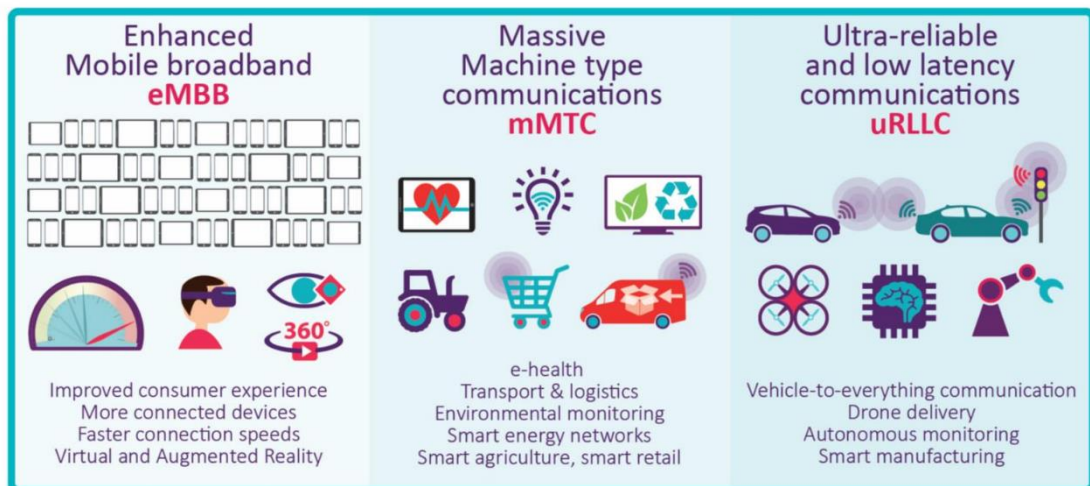 and security problems will need to be addressed, given the possibility of massive amounts of data being sent via a public network.

c. Ultra-Reliable Communications and Low Latency. 5G networks are designed to have very low latencies (network delays) and be more reliable. This qualifies them for a variety of applications, including driverless cars (in which cars communicate with one another, the road infrastructure, and even other road users) and smart manufacturing (connecting all the different machines in the production chain at various phases).

2.3   The Candidate Frequency Bands for 5G system

5G technology employs a wide spectrum range starting from less than 1 GHz to around 100 GHz. Furthermore, because of good propagation characteristics in this spectrum region, the lower frequencies provide better coverage. On the other hand, very high frequencies enhance transmission bandwidth, provide the most user capacity, and enable very high data rates. This makes them excellent for keeping everyone connected in crowded environments like stadiums. However, the International Telecommunications Union (ITU) has collaborated closely with local communication regulatory agencies to find the appropriate frequency bands for 5G services. This tedious work aims to allocate and identify harmonized spectrum worldwide to increase battery life, enable global roaming, reduce the complexity of mobile terminals, reduce cross-border interference, and increase spectrum efficiency. The possible bands for 5G are divided into two bands (Ancans, Bobrovs, Ancans, & Kalibatiene, 2017):

a.   Frequency bands less than 6 GHz: These frequencies range from sub-1 GHz to 6 GHz (mid-bands). This is identical to 4G, where the frequencies transmitted from cell phone towers are below 6 GHz.

b.   Frequency bands over 6 GHz: These frequencies are made up of mm-wave spectrum bands above 24 GHz.

5G deployment will rely on the mid-frequency spectrum as "primary bands" to support future system capacity. Spectrum at frequencies higher than sub-1 GHz will provide greater bandwidth, covering the capacity needed to serve many connected devices. Furthermore, these bands allow concurrently connected devices to operate at higher speeds (Ancans et al., 2017). Similarly, mm-wave frequencies provide several benefits for 5G, including large bandwidth that improves data rate, compact antenna size due to high frequencies, high-security short-range communication due to some high attenuation frequency bands, and reduced multipath effects relying on wideband spread-spectrum capability. Unfortunately, some fundamental constraints in the mm-wave bands must be addressed before commercial deployment (J. Zhang, Ge, Li, Guizani, & Zhang, 2016).

a. Weather conditions attenuate communications across these frequencies. This attenuation is raised by communication rage.

b. Normally, mm-waves typically have minimal network coverage in urban areas due to poor penetration. In inclement weather, the situation will deteriorate.

c. The antenna is tiny, and it requires more power for transmission and reception due to the small wavelength in mm-wave frequencies.

The MIMO technology compensates for the high attenuation facing 5G band frequencies to overcome these problems. However, such a solution is limited by the potential features of the present cellular phones: better screen- to-body ratios, larger battery sizes, and more popular wireless charging functions. As a result, 5G cellular phone designers must consider distances between antenna elements, antenna placement locations, and volumes (Huang, 2018). Additionally, the efficiency of the antennas, the ECC, and the isolation level will be considerable difficulties (Ban, Li, Wu, & Wong, 2016).

2.4   The MIMO Antenna for 5G

The MIMO technology is a well-established wireless communication method that enables the simultaneous transmission and reception of multiple data signals sent via a shared radio channel. Techniques of MIMO are widely used in Wi-Fi communications, 3G, 4G, and 4G LTE networks (Krumbein, 2016).

Massive MIMO, as the name suggests, involves utilizing MIMO technology on a much larger scale to increase network coverage and capacity. However, 5G New Radio goes one step further by introducing this idea. By using more transmitting and receiving antennas, massive MIMO improves transmission gain and spectrum efficiency. To achieve MA-MIMO capacity gain, multiple User Equipments (UEs) must create downlink traffic concurrently. The gain that MA- MIMO provides is really influenced by a number of factors (Sangodoyin & Molisch, 2018).

While there is no fixed number of antennas required for MA-MIMO applications, it is generally recognized that the system transmitting and receiving antennas should be more than eight each. And the number can be significantly larger; some systems use tens or even hundreds of antennas.

The MA-MIMO is essential for attaining the enhanced capacity and throughput increases promised by 5G, together with upgraded antenna methods like beamforming and beam steering. The International Mobile Telecommunications-2020 (IMT-2020) strategy calls for them to meet the 100x data rate and 1,000x capacity requirements (Chataut & Akl, 2020). The base station can transmit RF energy to the UE with more accuracy and efficiency because it employs a lot more antennas than the UEs in the cell, which results in a much narrower beam. While the channel information stays with the base station, the strength and phase of the antenna are independently controlled, simplifying UE by eliminating the need for numerous receiving antennas. A large number of base station antennas are added to the cell to improve the signal-to-noise ratio, which increases cell site throughput and capacity. Since mm-wave frequencies are used for 5G MA-MIMO, the necessary antennas are small and easy to install and maintain (Wallace & Jensen, 2004).

The mutual coupling issue, which occurs when the distance between the antennas is inevitable, is the main challenge with MIMO antenna systems. Mutual coupling, in general, describes the method by which a voltage is produced at the antenna terminals using the current surface-induced between adjacent antenna components (Wallace & Jensen, 2004). Increasing the separation distance between MIMO parts as a solution to the issue results in a larger system, which is not a desirable outcome. Numerous methods have been used to overcome this issue. For example,

a.   Neutralization Lines (NL) refer to a geometrical line that connects two antennas (S. Zhang, Pedersen, & letters, 2015).

b.   A decoupling network is a transmission line section with stubs that offers an additional signal path between array members, thereby canceling external coupling (C.-H. Wu, Chiu, Ma, & Letters, 2015).

c.   Electromagnetic Bandgap structures (EBG) mean that all polarization states and incident angles fall within particular frequency bands due to the periodicity of the artificial structures that aid electromagnetic wave propagation (Assimonis, Yioultsis, Antonopoulos, & Propagation, 2012).

d.   Ground plane adjustments, which refer to changes to the antenna structure's geometry in the context of miniaturization (Li, Luo, Yang, & Propagation, 2019).

e.   Meta surface walls remove surface waves by corrugating the antenna's sidewalls (Dadgarpour et al., 2016).

However, such a solution constrained by cost and complexity will negate the MIMO system's diversity advantages. Accordingly, the optimal design of a MIMO system using the polarization technique will prevent numerous difficulties in the frequency bands.

2.5   Polarization of Antennas

The polarization of antennas refers to "the polarization of the wave that is radiated by an antenna in the direction of maximum gain". A vector of an electric wave could be thought of as having two perpendicular components. Depending on the magnitude ratio

of the vector components and their phase difference, the form denoted by the vector sum of the two components at a fixed point in space may be a line, a circle, or an ellipse as time changes. Generally, one can write the instantaneous total electric vector (Et) as (Panahi, 2015):

$$E = \hat{X}\, Ex + \hat{Y}\, Ey,$$

(2.1)

where:

$Ex = E1\, co(wt - \beta z)$ is the horizontal component with amplitude $E1$,

$Ey = E2\, co(wt - \beta z \mp \delta)$ is the vertical component with amplitude

$E2$ and a phase difference δ by which EY leads / lags EX.

2.5.1 Linear Polarization

A traveling wave is considered to be LP if the phase difference between the wave vector's two orthogonal components is zero, i.e., $\delta = 0°$. Then, depending on the component magnitude, a linearly polarized wave is formed in the vertical, horizontal, or any plane between them. For example, if $E1 = 0$, it is vertical linear polarization, if $E1 = E2$, it is 45° tilted LP as seen in figure 2.3.
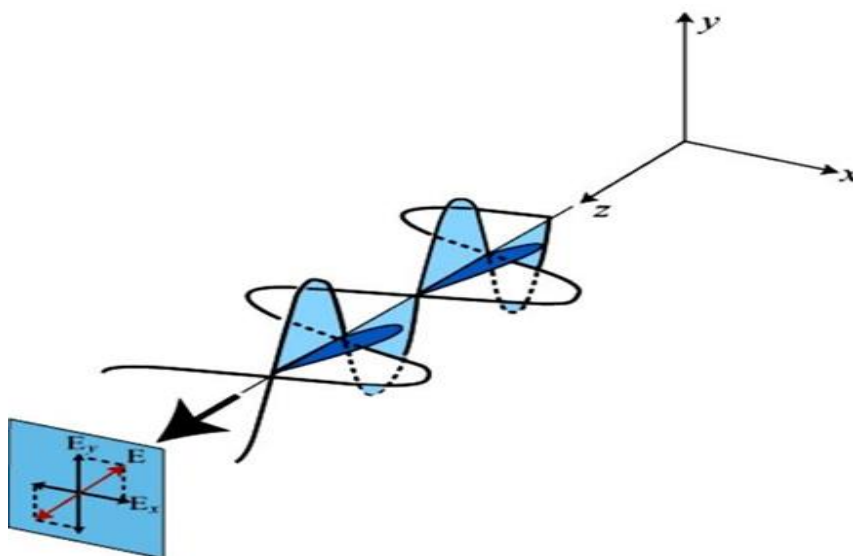

Figure 2. 3 An LP wave with a 45° orientation (Panahi, 2015)

2.5.2 Circular Polarization

when $E1 = E2$ and $\delta = \pm 90°$ A wave has a CP. When the angle is $-90°$, the wave is circularly polarized in the right direction; when the angle is $+90°$, the wave is circularly polarized in the left direction. As shown in figure 2.4, there are two orthogonal waves with a phase difference of 90°, a sine (XZ plane) and a cosine (YZ plane), form a Right Hand Circularly Polarized (RHCP) in the (Z) direction over time.
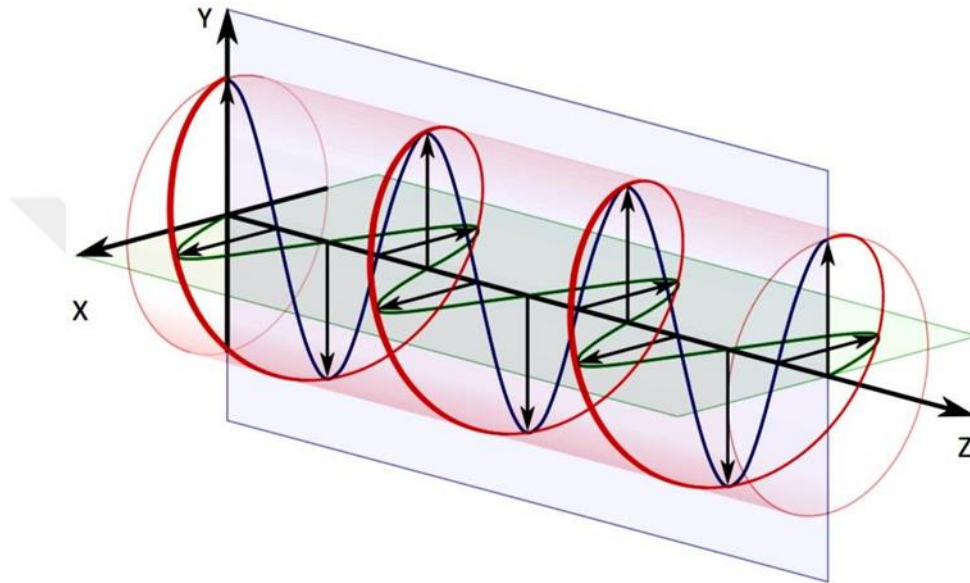

Figure 2. 4 Right-hand circular polarization (Panahi, 2015)

2.5.3 Elliptical Polarization

when $E1 \neq E2$ and $\delta \neq 0$, a wave has elliptical polarization. As with circular polarization, elliptical polarization can be right-handed (clockwise) as shown in figure 2.5, or left-handed (anti-clockwise).
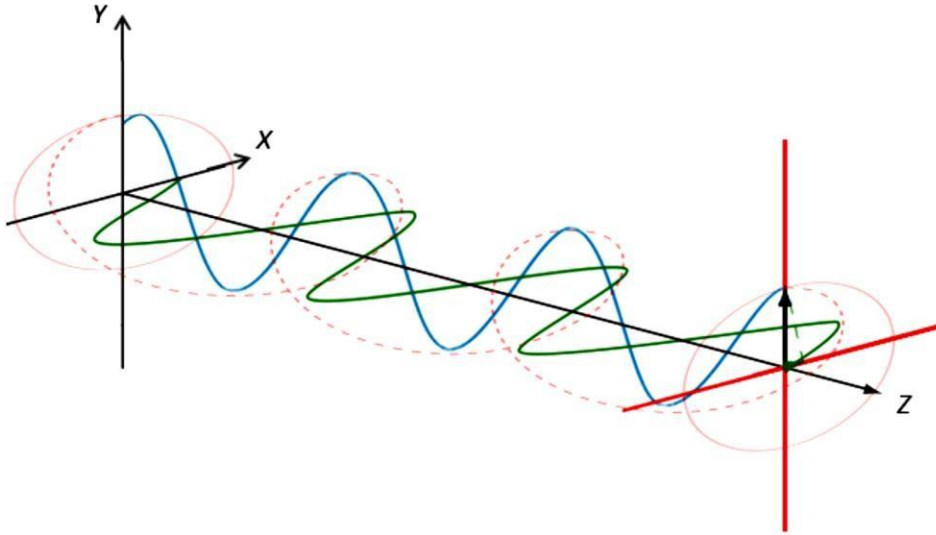
Figure 2. 5 Right-hand elliptical-polarization (Panahi, 2015).

Linear polarization is a relatively simple process utilized in mobile phones, radio broadcasting, and a variety of other traditional radio applications. CP, on the other hand, possesses special features that make it ideal for high-performance radio systems. Because polarization mismatch is a possibility, polarization is essential for wireless communication. Due to reciprocity, an antenna uses the same polarization for both transmission and reception. As a result, a vertically polarized antenna cannot communicate with a horizontally polarized antenna (linear polarization parallel to the ground) (linear polarization perpendicular to the ground). Therefore, for best reception in an RF communication system, the receiving antenna should have the same polarization as the transmitting antenna (Fan, 2018). The power loss due to polarization mismatch is calculated using the Polarization Loss Factor (PLF), which can be denoted by: (Fan, 2018). The angle β represents the acute angle between the polarization directions of two linearly polarized antennas, and the PLF is denoted as follows:

$PLF = cos^2(\beta).$

(2.2)

If $\beta = 0$, both antennas will have the same polarization, and no power loss will occur as a result of the polarization mismatch. If $\beta = 90°$, the receiving and transmitting antennas' polarizations will be perpendicular; there will be no connection between these two antennas, as they are unable to receive power from one another. As a result, the

benefit of a CP antenna is that signals sent between them will not suffer from polarization mismatch loss if both antennas have the same circular polarization. Furthermore, the reciprocity theorem dictates that a signal from a Left Hand Circularly Polarized (LHCP) antenna cannot be received by an RHCP antenna. Circular polarization also has another benefit because an RHCP wave will convert to an LHCP wave upon reflection. The reflected wave will not interfere with the desired incoming wave. So, CP antennas exhibit some resistance to the multipath effect. Thus, the current thesis attempts to employ this method (Gao, Luo, & Zhu, 2014a).

2.6   Antennas of CP Microstrip Patch

The most used CP antenna shape is undoubtedly microstrip patch antennas. They consist of a dielectric PCB with a ground plane printed on one side and a conducting patch (which acts as a resonator) printed on the other. Contrary to certain antennas (such crossed dipoles), the insertion of the orthogonal mode has no impact on patch size. To manage input resistance, the breadth should be about equal to the length even for linearly polarized antennas. The categorization of the microstrip patch of CP structures-single feed or multiple feeds-determines the CP production technique. These classifications are addressed in greater detail in (Narbudowicz, 2013).

2.6.1 Single-fed CP Patch

The use of a single feed provides the advantage of a smaller feed network and simplicity, as phase shifters and power dividers are not required. However, this implies that the antenna geometry must generate the phase shift and two orthogonal modes, which are necessary for CP (Narbudowicz, 2013). There are numerous ways to accomplish this, the most popular of which is seen in figure 2.6.

Figure 2.6(a) shows the feed that is situated on the patch's diagonal to excite two modes using the almost-square patch technique. The phase difference is created by altering the patch's length and width slightly, causing the two modes to resonate at slightly different frequencies. Around the resonant frequency, the antenna's performance changes from capacitive (bottom half of the Smith chart) to inductive reactance (upper part of the Smith chart). Thus, between the two resonances' frequency ranges, one mode will have a positive reactance while the other will have a negative one. A 90° phase shift can be

18

achieved by altering this value. This is accomplished by adding a slight difference (Δ) between the length and width of the patch (Narbudowicz, 2013).
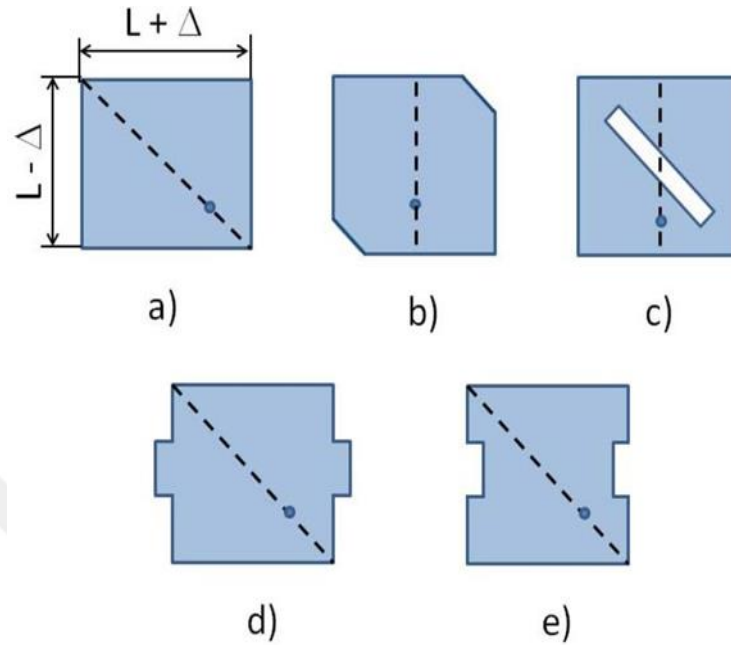

Figure 2. 6 Various CP patches geometries; the dashed line indicates the location of the feed point (Narbudowicz, 2013).

The truncated corner method, which entails cutting off two of the rectangular patch's diagonally opposed corners, is shown in Figure 2.6 (b). A feed is located in the middle of one of the edges. As a result, one mode is immediately aroused, and the other is triggered by an imperfection in the square geometry of the patch. Solutions for polarization reconfigurability have been proposed by covering and uncovering the truncation, as discussed in (Hsu, Chang, & letters, 2007), as the sense of polarization is controlled by which two corners are truncated. When feeding the patch straight from a 50W microstrip line for these antenna types, it can be challenging to get a suitable impedance match. An inset feed can be used with linearly polarized antennas. However, the two slots generated by this technique disturb the current in the orthogonal mode, hence degrading circular polarization. In (Kavas & Kırık, 2016) presented a solution to this problem. The inset feed's impact is balanced by extra slots cut along the patch's other edges, which results in an excellent AR performance when fed directly from a

50Ω microstrip line. Alternatively, a diagonal slot can be added to the patch to replace the truncated corners, as seen in figure 2.6(c), comparable to a truncated corner. With the appropriate phase shift, the narrow slot divides the energy into two orthogonal modes. Finally, a projecting stub from the edge or a part deleted from the edge, as shown in figures 2.6(d) and 2.6(e) respectively, or a combination of the two can be employed to produce a 90° phase shift. When appropriately designed, these structures introduce capacitance and inductance that create a phase shift (Narbudowicz, 2013).

2.6.2 Dual-fed CP Patch

Figure 2.7 shows a straightforward CP microstrip patch antenna that was built using the dual-feed approach from the antenna's top and side perspectives. Accordingly, in figure 2.7(a), a square microstrip patch is supplied with two orthogonal microstrip feedlines, which excite the patch antenna in the TM01 and TM10 modes, in order to achieve circular polarization. As a result, it emits waves that are both horizontally and vertically polarized (Gao, Luo, & Zhu, 2014b). In order to establish a 90° phase difference between two orthogonally polarized waves, a microstrip hybrid is also used. Figure 2.7 shows a side view of the antenna (b). The metallic patch is etched into the top of a dielectric substrate with a thickness of (h) and a relative permittivity of (εr). A metallic ground plane is used on the dielectric substrate back. To construct an antenna that is resonant at a frequency ($f°$), the patch's length (L) can be approximately calculated as:

$$L \approx \frac{c}{2f\circ\sqrt{\frac{\varepsilon_r+1}{2}}},$$
(2.3)

where (c) is the speed of light. To assure the correctness of antenna designs, full-wave electromagnetic simulators may be used to optimize and model the antenna's dimensions. You can use the answer to equation (2.3) as the starting point for the antenna optimization procedure.
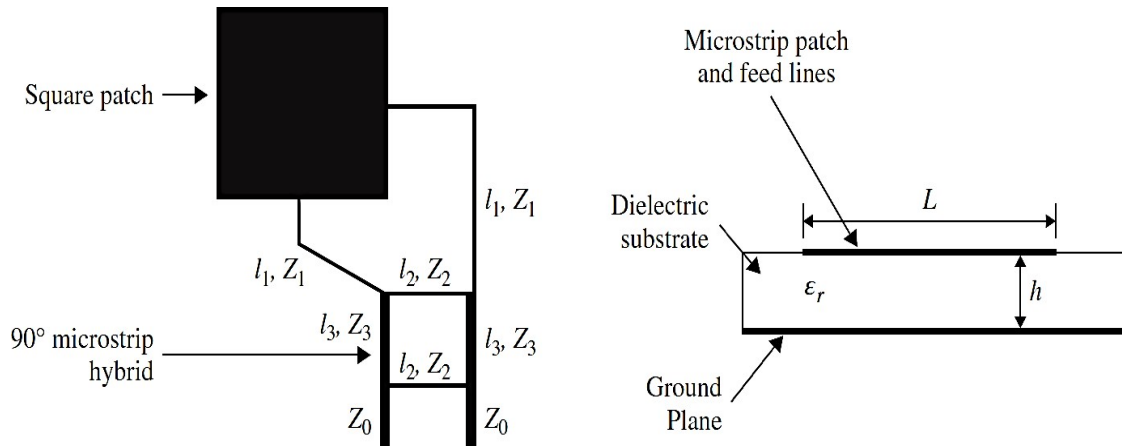
Figure 2. 7 A microstrip line-feed patch antenna with a 90° hybrid (Gao et al., 2014b).

Polarizer and power divider requirements for dual-fed patch antennas increase the antenna's complexity and size. The advantage is that because it is independent of the mode perturbing element, the axial ratio bandwidth is enhanced. Depending on the bandwidth characteristics of the phase shifter, the antenna's axial-ratio bandwidth may be as big as the impedance bandwidth.

The square patch and the two ports of the microstrip 90° hybrid are connected by two microstrip feed lines, as seen in figure 2.7(a). The microstrip line acts as an impedance transformer between the antenna's input and the hybrid's input ports. The characteristic impedance (Z1) and the length (l_1) of the microstrip feed lines can be calculated by (Gao et al., 2014b):

$$Z_1 = \sqrt{Z_{in} Z_o} \, , \tag{2.4}$$

$$l_1 = \frac{\lambda_g}{4} \, , \tag{2.5}$$

where, (Zin) is the patch antenna input impedance, (Z0) is the microstrip line characteristic impedance at the hybrid circuit input, and (λg) is the microstrip line guided wavelength.

The microstrip 90° hybrid circuit is composed of four microstrip line sections. The width and length of each section of microstrip lines can be determined using the following equations (Gao et al., 2014b):

$$l_2 = l_3 = \frac{\lambda_g}{4},$$

(2.6)

$$Z_2 = Z_\circ,$$

(2.7)

$$Z_3 = \frac{Z_\circ}{\sqrt{2}},$$

(2.8)

where l_2 and l_3 denote the microstrip line length, (Z_2) and (Z_3) denote the microstrip line sections characteristic impedance also indicated in figure 2.7(a).

The characteristic impedance of the microstrip line at the hybrid circuit's input, ($Z0$), is typically 50 Ω. Circuits of microstrip hybrid are simple to build and are frequently utilized in CP antennas. One disadvantage of the microstrip hybrid circuit is its large size. Additionally, the CP patch antenna can be fed through probe feeds, electromagnetically coupled feeds, slot coupled feeds, or Coplanar Waveguide (CPW) feeds. In figures 2.8 and 2.9, a CP patch antenna with two probe feeds and a CP patch antenna with slot-coupled feeds are shown, respectively (Gao et al., 2014b).
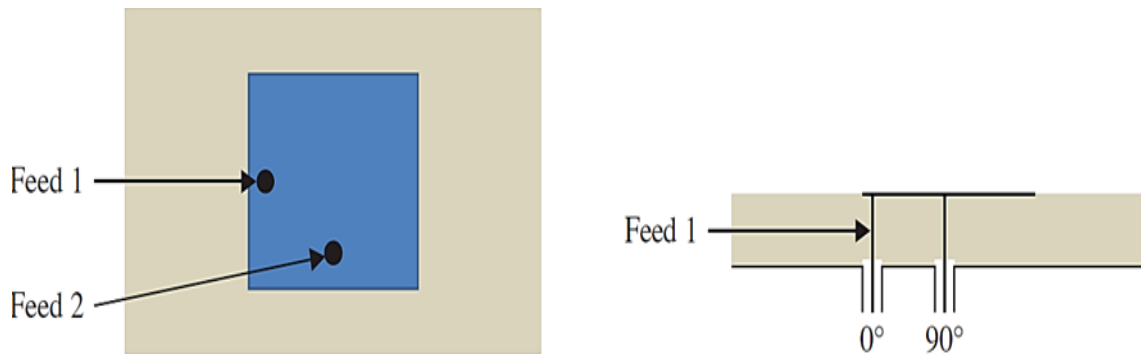

Figure 2. 8 a patch antenna for probe-feed with an external phase shifter of 90 degrees (Gao et al., 2014b).
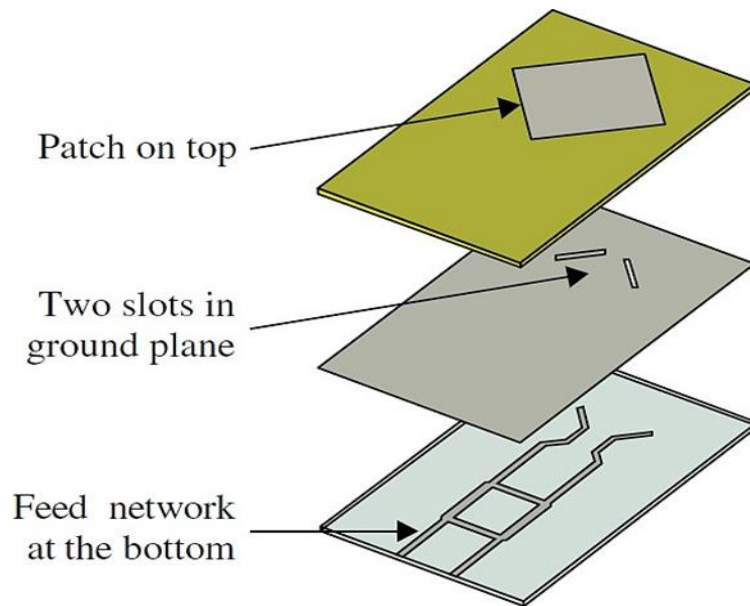
Figure 2.9 Patch antenna with a slot-coupled CP (dual feed with a hybrid coupler) (Gao et al., 2014b).

2.7 Antenna Parameters

The performance of the antenna is evaluated using a variety of different criteria. Naturally, each antenna is designed for a specific application, and hence each parameter significance differs with each design. However, the following parameters are typically measured:

2.7.1 Voltage Standing Wave Ratio, Return Loss, and Reflection Coefficient

The characteristic impedance of the transmission line linked to the antenna's feed point must match the input impedance of the antenna. The antenna is typically fed by a 50 cable. In order to prevent an impedance mismatch at the antenna feed point, the antenna input impedance must be equal to 50. Signal reflections take place when there is an impedance mismatch, which causes part of the signals sent to the antenna to be reflected back to the signal sources (Simone, Fanti, Lodi, Pisanu, & Mazzarella, 2021).

The reflection coefficient (Γ) expresses the ratio between the reflected and incident wave voltages. The following equation can be used to link the reflection coefficient at the antenna's feed point to the antenna's input impedance:

$$\Gamma = \frac{Z_{in} - Z_0}{Z_{in} + Z_0} .$$

(2.9)

(Zin) and (Zo), denote the antenna's input impedance and the transmission line's characteristic impedance connected to the antenna feed point, respectively. As demonstrated in equation (2.9), if Zin = Zo, the reflection coefficient is zero. Return loss (measured in decibels) is defined as:

$$RL = -20 log \ |\Gamma|.$$

(2.10)

The needed return loss for a well-designed antenna is typically at least 10 dB, while some antennas on tiny mobile terminals only reach around approximately 6 dB (Gao et al., 2014b). The VSWR is the ratio between the transmission line's maximum voltage ($Vmax$) to its minimum voltage ($Vmin$). It is defined as follows:

$$VSWR = \frac{|V_{max}|}{|V_{min}|} = \frac{1 + |\Gamma|}{1 - |\Gamma|} .$$

(2.11)

2.7.2 Fractional Bandwidth

Normally, an antenna is designed to work over a certain frequency range. Thus, impedance bandwidth can be described as "the frequency range difference between the upper ($fhigh$) and lower (flo) frequencies when (S11$\leq$ -10 dB)". In this context, the impedance bandwidth is often normalized to the bandwidth's center frequency (fc), it is referred to as the "Fractional Bandwidth (FBW)" in this situation and can be represented as [52]:

$$BW = f_{high} - f_{low.}$$

(2.12)

2.7.3 Radiation Pattern, Gain, Directivity, and Efficiency

The antenna's radiation pattern depicts the radiated power distribution throughout space. It can be represented as the radiated power versus the elevation angle (θ) or the azimuth angle (φ) in a spherical coordinate system. While it provides essential

24

information about an antenna's angular characteristics. It does not provide information about the actual amount of power radiated. A crucial factor called directivity (D) is defined as "the ratio of the highest radiation intensity of the proposed antenna to the isotropic radiation intensity." The total power emitted by an antenna per unit solid angle is referred to as the radiation intensity (U) of an antenna. In purely mathematical terms:

$$D = \frac{4\pi U_{max}}{P_{rad}} .$$
(2.13)

Where, U_{max} is the maximum radiation intensity, P_{rad} is the radiated power in watts. The gain (G) of an antenna is defined as the ratio of the designed antenna's radiation intensity in the desired direction to the isotropic radiation intensity. The gain of an antenna is identical to the directivity, although it includes the antenna's efficiency (η), as some power is wasted in the antenna.

$$G = \eta \cdot D.$$
(2.14)

Gain and directivity are typically measured in decibels. Antenna gain is frequently expressed in terms of dBi, indicating that it is determined in relation to an isotropic radiator (Al-Ani, Al-Ani, Mosleh, AbdAlhameed, & Science, 2020).

2.7.4 Axial Ratio

The AR is the ratio of the ellipse's major to minor axes, and it is equal to:

$$AR = \frac{a}{b}.$$
(2.15)

where the main axis is (a) and the minor axis is (b). It is challenging to obtain in reality AR = 1 or 0, which is the case with circular polarization. Since complete circular polarization is really impossible to achieve, an ellipse is typically used to represent the curve traced as a function of time at a particular place. Typically, CP antennas require AR to be less than 3 dB.

2.8 Benefits of CP

Circular polarization has several advantages over linear polarization, as detailed below:

1. **Resistance to Faraday Rotation:** The Faraday effect makes the polarization plane rotate. The magnetic field component in the propagation direction is proportional to this rotation. This presents an issue in the upper parts of the Earth's atmosphere, where massive magnetic fields are generated by highly ionized plasma (Z. Wu, Yang, Sun, & Science, 2022). However, this field strength varies considerably, depending on many difficult-to-predict variables (i.e. solar activity, time of the day, year, etc.). For LP, this would result in a signal polarization mismatch. CP is immune to this effect since both orthogonal components have identical magnitudes and are rotated at the same angle. This is the primary reason for the widespread use of CP in nearly all Earth– satellite communication systems.

2. **Multipath:** multipath occurs when the primary signal and the reflected signal arrive at the receiver almost simultaneously. The use of CP enables the antenna system to filter out signals arriving via several paths (Garcia et al., 2012). This can occur as a result of a certain circular polarization sensation reflecting with a different sense following wave incidents on conducting flat surfaces (i.e. a right-handed CP wave transforms into a left-handed CP wave and vice versa).

3. **Loss due to misalignment:** in linearly polarized communication systems, the transmitting and receiving antennas must be aligned to minimize polarization mismatch losses. Because the LP wave is received regardless of its orientation in a CP antenna, alignment is not required (Jebbawi, Egels, Pannier, & Letters, 2020).

CHAPTER THREE

SINGLE HEXAGON ANTENNA

3.1 Introduction

The "Federal Communication Commission" of the United States has granted permission for the utilization of ultra-wideband (UWB) technology in frequency bands between (1 to 10.6 GHz). The key research goals in "commercial" and "military" applications, respectively, are the very tiny size and reduced cost. Ultra-wideband technology, which also enables users to wirelessly link a large number of devices and a large number of users in the areas of dispatch and reception, eliminates the need for cables for users of wireless systems. This chapter suggests an ultra-wideband (UWB) printed monopole microstrip antenna with a hexagon slot that is 20 by 16 millimeters square. The tiny, thin, and planar UWB antenna, which has two hexagon slot radiators and is provided with a single 50 micro-strip line with a smaller ground plane, has stimulated the coaxial connection of the SMA. The antenna also features a smaller ground plane.
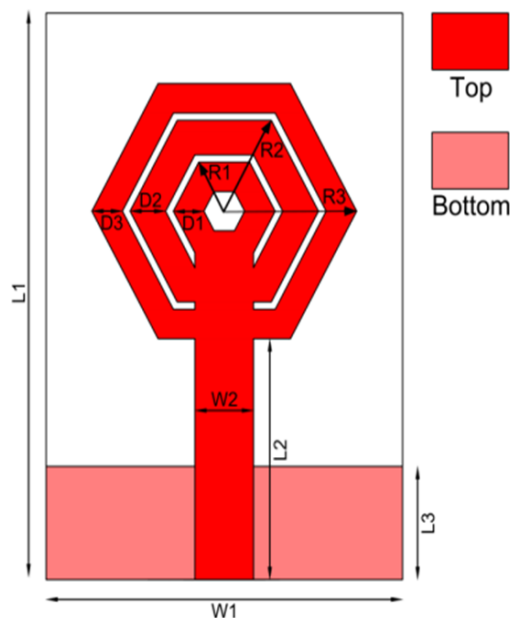
Figure 3. 1   Proposed single
hexagonal-shaped monopole antenna.

To achieve a dual-band, the sizes of each ring and ground plane are tuned. Also, R1, R2, and R3 are the inner, middle, and outer ring radii (plural of 'radius'), and D1, D2, and D3 are their corresponding widths. All optimized parameters marked in Figure 1 are listed in the Table 3.1.

Table 3. 1 Antenna parameters Values

Parameter	Value (mm)	Parameter	Value (mm)
L1	20	R2	3.7
W1	14	R3	5.2
L2	8.5	D1	1.2
W2	2.3	D2	1.4
L3	4	D3	1.2
R1	2	h	1.6
Wg	18	hc	0.035

3.2. Design Steps of Hexagon Patch Antenna

A hexagon antenna part (unit cell) was built with a dimension of $16 \times 20 \times$ The $16 \times 20 \times 1.6$ mm^3 hexagon antenna portion (unit cell) was constructed. Three levels make up the suggested model; the first is the patch layer, and the second shows how the patch layer and ground layer are separated from one another. The FR-4 substrate layer has a 1.6 mm thickness and has a permittivity of 4.4 and a tangent loss of 0.035. The third layer serves as partial ground and consists of a 50- rectangular microstrip feed line connected to the power supply and a 50- rectangular microstrip that increases fractional bandwidth through a SMA connection. The specifics of the single antenna's geometry, as shown in figure 3.1, and its design parameters are listed in Table 3.1. But, as an operating frequency and substrate characteristics function, the resonant length of a microstrip patch may be calculated using straightforward effective relative dielectric constant calculations, as illustrated below:

$$\varepsilon_{reff} = \frac{\varepsilon_{reff}+1}{2} + \frac{\varepsilon_{reff}-1}{2}\left[1 + 12\frac{h}{W}\right]^{\frac{-1}{2}} , \tag{3.1}$$

$$W = \frac{c}{2f}\sqrt{\frac{2}{\varepsilon_r+1}} , \tag{3.2}$$

$$L_{eff} = \frac{c}{2f\sqrt{\varepsilon_{reff}}} , \tag{3.3}$$

$$\Delta L = 0.5h , \tag{3.4}$$

$$L = L_{eff} - 2\Delta L , \tag{3.5}$$

where ε_{reff} effective isolation constant, ε_r effective dielectric constant, L_{eff} effective length of resonant patch antennas, ΔL represent the width difference, L_{eff} effective length, L stands for the length of resonant patch antennas, W for their width, and c for the speed of light in empty space. There have been suggestions for tweaks to this patch that would increase its usable bandwidth. The patch close to the micro-feeding strip's line has been tapered as a preliminary adjustment. Due to the tapering effect of the component connected to the micro-strip line, the simulations have adjusted the patch dimensions such that the length is now 20 mm and the width is now 16 mm, as shown in Table (3-1). When those parameters are applied, the suggested antenna is found to have a usable frequency range (VSWR 2) between 3 GHz and 5 GHz, making it a promising contender for usage in UWB applications.

3.3. Parametric Study of Proposed Hexagon Patch Antenna

In order to achieve the required UWB frequency range, parametric research is performed on several design factors that impact the electrical execution of antenna. Since the default antenna settings don't provide the highest possible performance, optimizing the antenna requires experimenting with different settings until the ideal one is found.

3.3.1. Parametric Analysis of Multi Hexagon   Patch Antenna Proposed

This section gives a parametric analysis of a multi-hexagon patch ultra-wideband antenna, since the geometric parameters have a considerable effect on antenna

29

performance. The feed transmission line size, ground plane size, and slot size have all been mapped out on a design curve for a range of band frequencies. It has been thought about how many of them there are, and what percentage of them there are, in addition to the other bandwidth options. These configurations have been evaluated to ensure that the degree bandwidth and radiation designs are consistent with the predicted outcomes.

A. Substrate Length Effect (L)

The parametric analysis of antenna length is presented in this part as the initial design parameter for antennas. However, the antenna substrate length is simulated to show how the suggested antenna design would vary as the antenna length changes. The reflection coefficient (S-parameter) is illustrated in Figure 3.2 where S11 value is obtained with a length of 20 mm at center frequencies of 3.3 GHz and 4.5 GHz of less than -10 dB. It is clear that the antenna substrate length have effective impact on the performance of the antenna design.
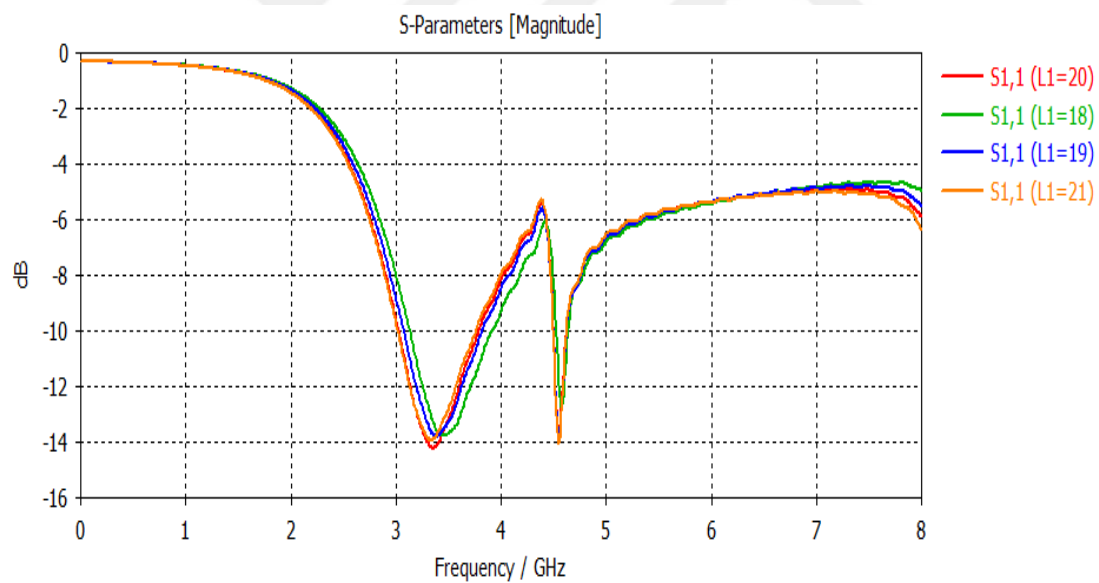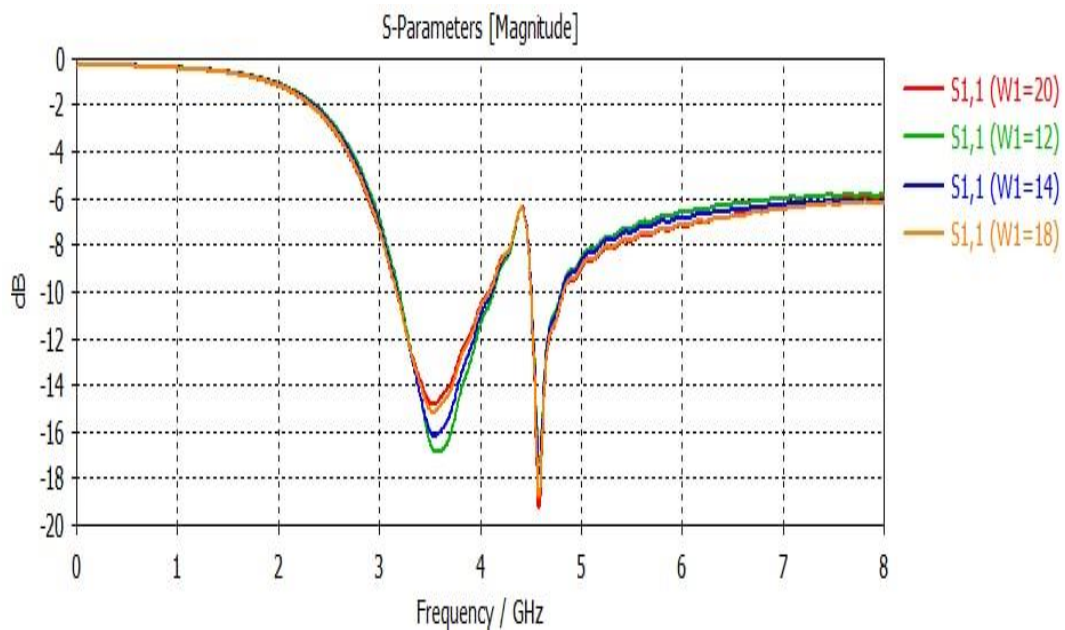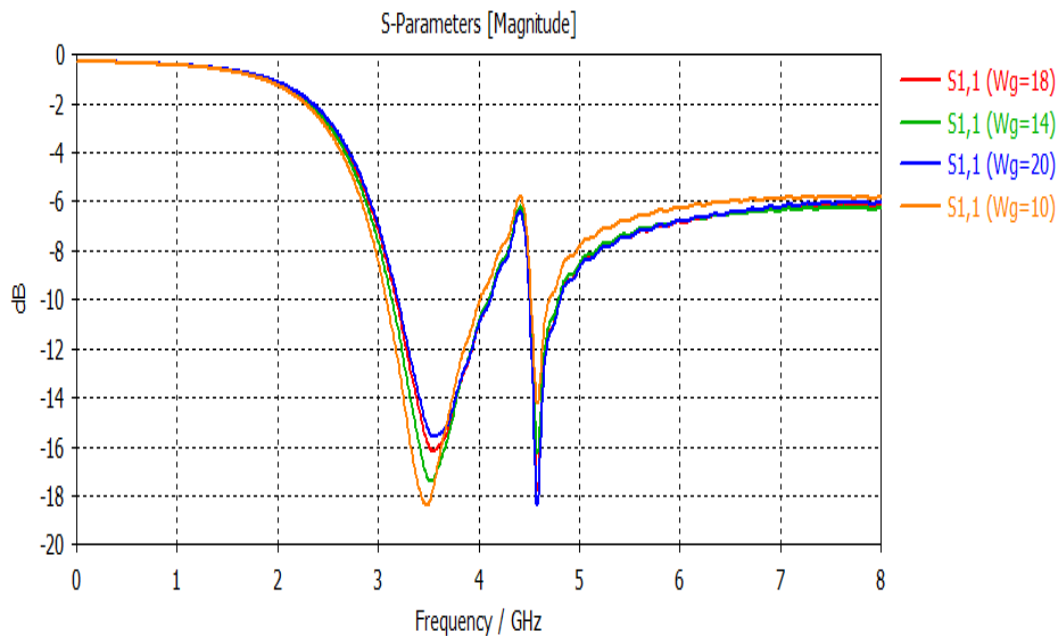

Figure 3. 2 Simulation S-parameter against frequency for a multi hexagon patch antenna at various values of (L)

B. Effect of Substrate width (W1)

The impact of substrate width variation has been researched and assessed. Figure 3.3 depicts the frequency change with various substrate length values. At the center frequencies of 3.3 GHz and 4.5 GHz, the effective substrate width with the best S-parameter value was attained with a length of 18 mm and a reflection coefficient of less than -10 dBm. For more discussion the substrate width less than 18 mm or more that 19 mm has negative effect on antenna performance.
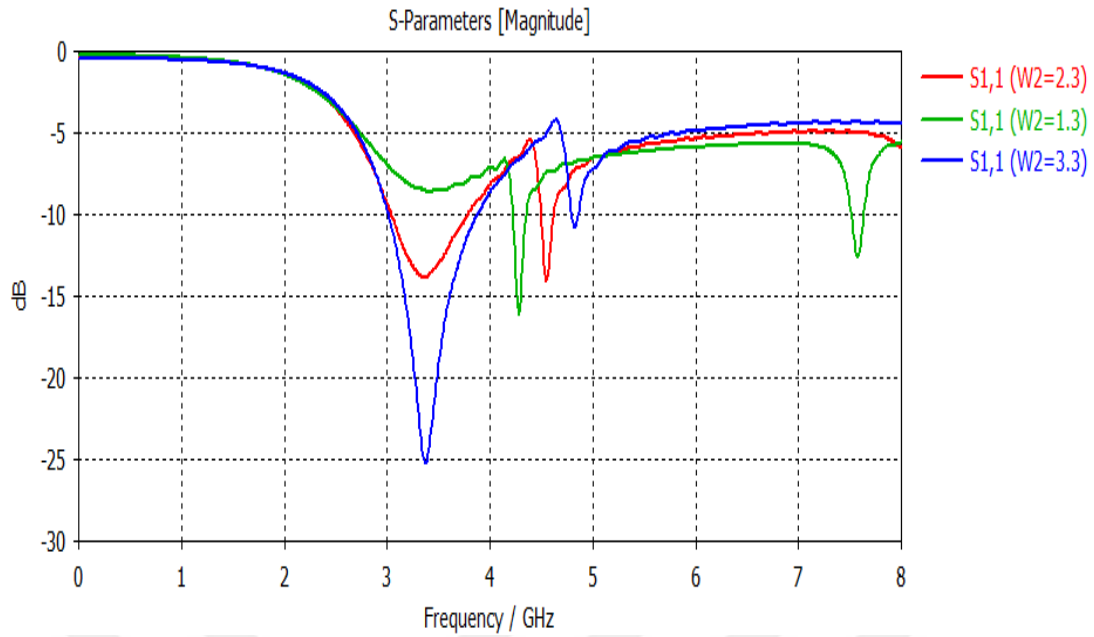

Figure 3. 3 Simulation S-parameter against frequency for a multi hexagon patch antenna at various values of (W)

C. Effect of the ground width of a hexagon antenna (Wg)

This parametric analysis evaluates the suggested antenna's width. The influence of altering ground width on reflection coefficient could be seen in Figure 3.4. As seen in the figure, the 18 mm ground width was attained with a reflection coefficient that was less than -10 dB and a center frequency of 3.3 GHz and 4.5 GHz. The 18 mm ground width with the lowest value of the reflection coefficient is the ideal ground antenna

width. However, the antenna ground width with less than 18 mm or greater than 18 mm can show negative effect on antenna performance.

Figure 3. 4 Simulation S-parameter against frequency for a multi hexagon patch antenna at various values of Wg

D. Influence of Feeder Width Strip (W2))

To demonstrate the impact of feeder width variation on the performance of the suggested antenna, the feeder width has been simulated in this parametric analysis. The link between the "S-parameter" and the antenna strip feeder width is shown in Figure 3.5. At the center frequencies of 3.3 GHz and 4.5 GHz, it is demonstrated that an antenna strip with a width of 3.3 mm produces the lowest reflection coefficient value less than -10dB.

Figure 3. 5 Simulation S-parameter against frequency for a multi hexagon patch antenna at various values of (W$_2$)

E. Effect of the Hexagon radius (R3)

The center of the antenna strip models, which are simulated and studied as a variant on the antenna design, has a radius of R3. As shown in Figure 6, the best value of central radius of R3=5.2 mm offers a bandwidth of 3.3 GHz and 4.5 GHz at S11-10 dB. The appropriate hexagon radius cannot be less than the 5.3 mm because it will decrease the antenna performance as presenting in Figure 3.6.
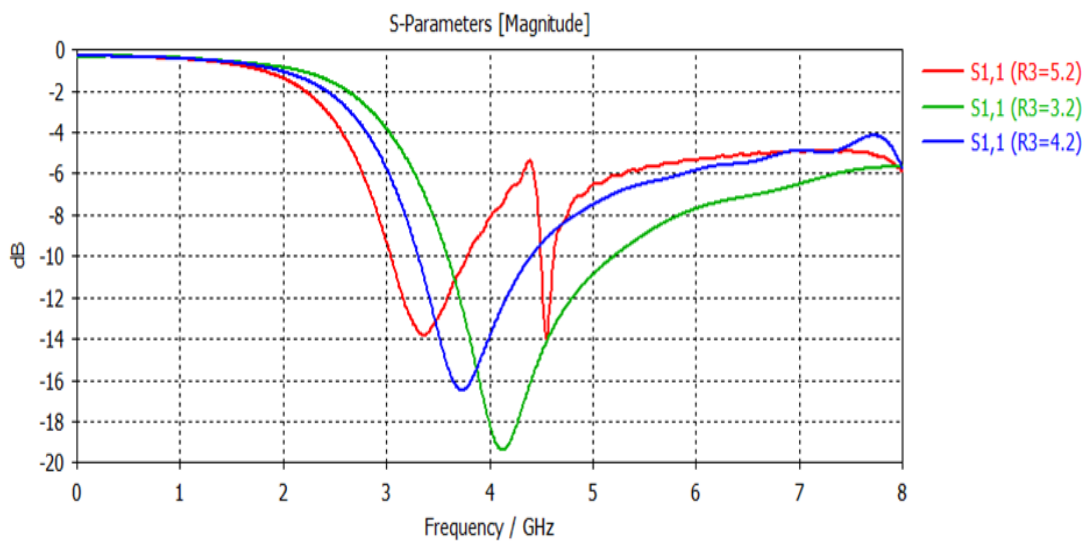
Figure 3. 6 Simulation S-parameter against the radius of central hexagon (R3)

3.3.2. Characteristics of Hexagon Patch Antenna

Let's now sketch up the proposed antenna's features using the best possible parameter values:

A. Gain of the Antenna

Figure (3-7) below shows the simulation results for the proposed hexagon patch antenna. The curve indicates that the maximum gain is (2.1 dB) at 3.36 GHz.
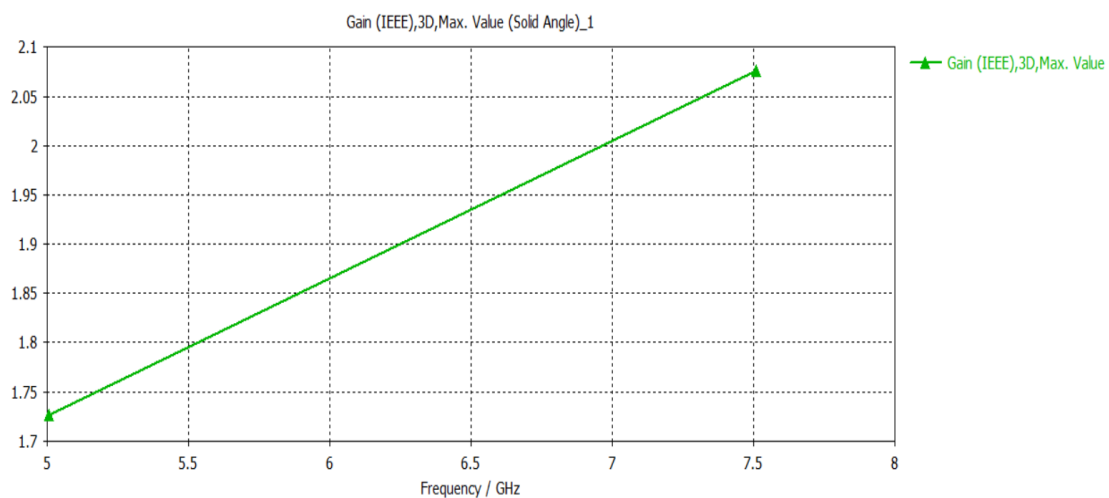
Figure 3. 7 Gain of a hexagon Patch Antenna

B. S-parameter

Fig. displays the antenna's S-parameter in relation to frequency (3-8). The suggested antenna can operate in the frequency range of based on the measured results of (3 GHz to 5 GHz). Several technologies, including WLAN, Wi-Fi, HIPERLAN-2, INSAT, the Radio Astronomy Band, and STM, operate in this spectrum.
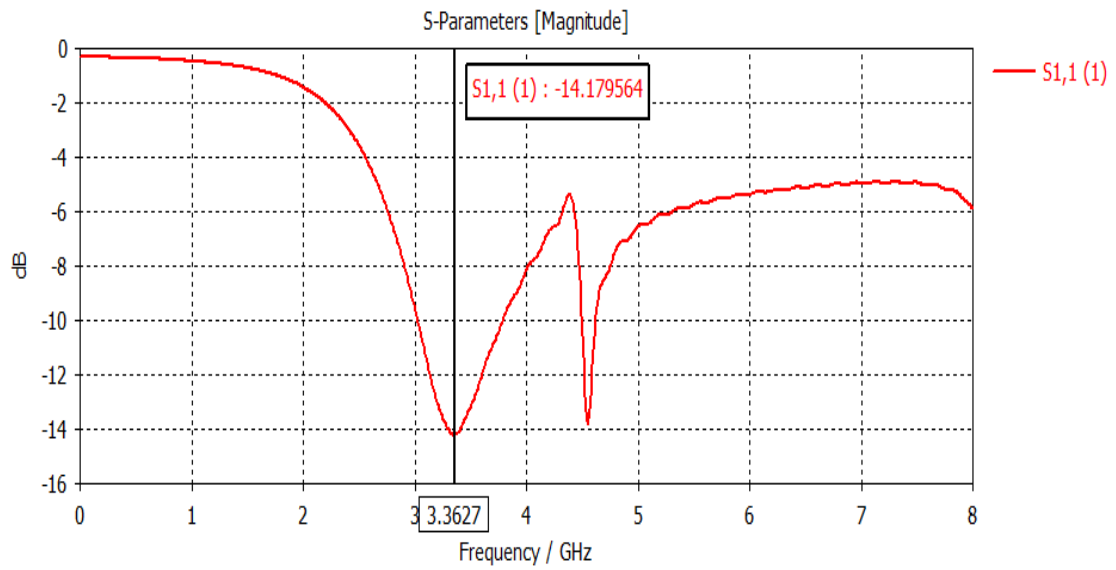
Figure 3. 8 Simulation S-Parameter against frequency for a multi hexagon patch antenna

C. "Voltage Standing Wave Ratio" (VSWR)

Figure (3-9) displays a VSWR vs. frequency plot for the antenna, and it is clear that the values are within acceptable bounds for the entire band attained.
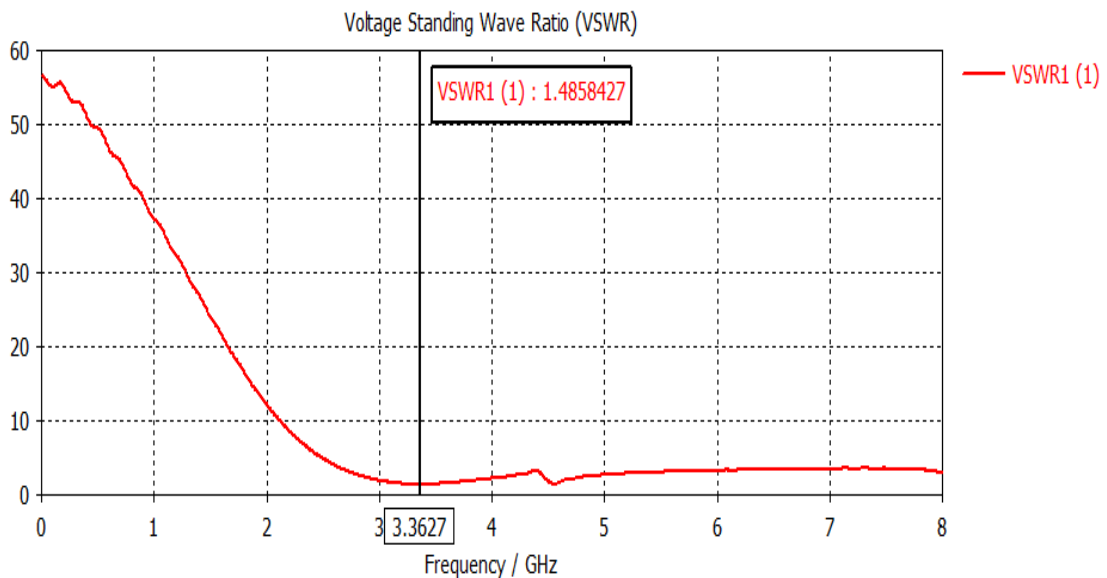

Figure 3. 9 Simulation VSWR against frequency for an multi hexagon patch antenna

D. Current Distribution

Figures 3-10 show antenna current distributions at 3.36. Maximum currents at 3.36 GHz and 7.6 GHz are depicted in Figures 3-10.

surface current (f=7.611) [1]
Frequency   7.611 GHz
Phase   0°
Maximum (Plot)   90.1084 A/m
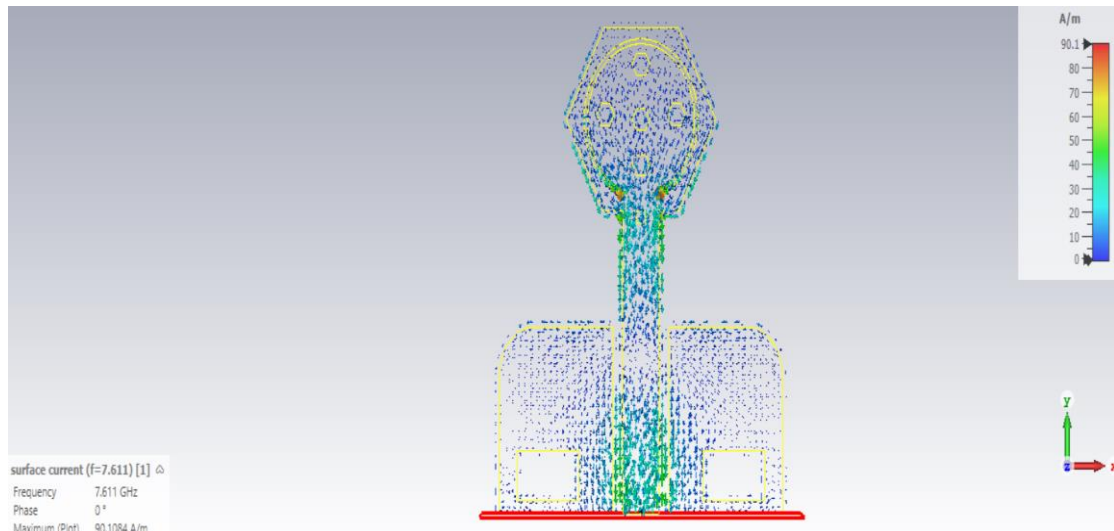
Figure 3. 10 Current distributions at both frequencies 3.36 GHz .

E. 3D Radiation Pattern

We will illustrate the 3D radiation at 3.36 GHz in Fig. (3-11). In this image, maximum directivity at 3.36 GHz is displayed as 4.64 dB, Clearly, one of the goals of these designs is to increase bandwidth, a feature that is required in many situations.
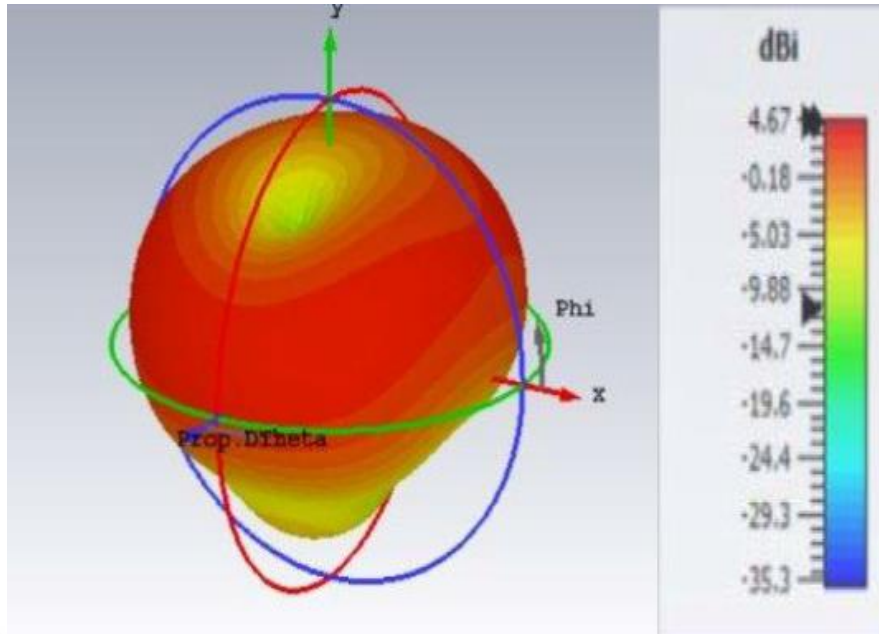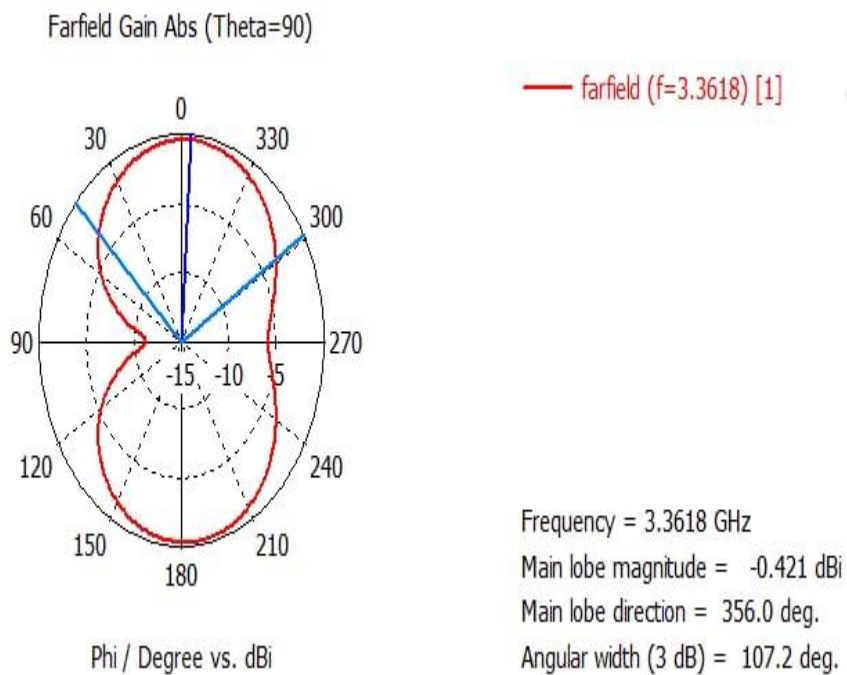
Figure 3. 11 3-D radiation pattern for a multi hexagon patch at various values of frequencies 3.36 GHz

F. Far filed Radiation Patterns

The radiation patterns in the Figure 3.12 the "y-z" (E-plane) and "x-z" (H-plane) planes, the enhanced antenna was modelled for two frequencies in the passband that are equal to (3.36 GHz). The E-plane and H-plane are displayed (The main lobe magnitude of the H-filed signal is 0.88 dBi in the direction (150.0), while the angular breadth of the H-filed signal is 356. In contrast, the main lobe magnitude of the E-filed signal is 0.88 dBi.

Farfield Gain Abs (Phi=90)

—— farfield (f=3.3618) [1]

Frequency = 3.3618 GHz
Main lobe magnitude = 0.884 dBi
Main lobe direction = 159.0 deg.
Angular width (3 dB) = 100.4 deg.
Side lobe level = -2.3 dB

Theta / Degree vs. dBi

(a)

Farfield Gain Abs (Theta=90)

—— farfield (f=3.3618) [1]

Frequency = 3.3618 GHz
Main lobe magnitude = -0.421 dBi
Main lobe direction = 356.0 deg.
Angular width (3 dB) = 107.2 deg.

Phi / Degree vs. dBi
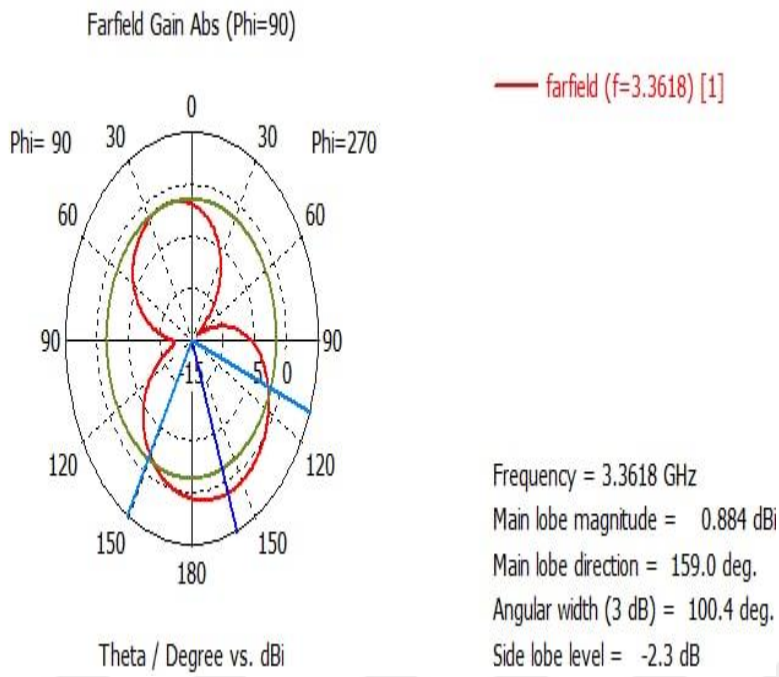
(b)

Figure 3. 12 Eclectic field at 3.36 GHz, (b) Magnetic field at 3.36GHz

CHAPTER FOUR

PROPOSED MIMO HEXAGON ANTENNA

4.1. Introduction

In this chapter new MIMO hexagon antenna proposed for Ultra-wideband (UWB) applications is presenting. The new MIMO antenna proposed for the application of both Wi-Fi and WiMAX. Measurements show that the proposed antenna radiates in both an omnidirectional H-plane design and a bidirectional E-plane design over the whole range of frequencies that make up the UWB band. The proposed antenna's tuning control and its radiation properties are examined in depth.

4.2 Modeling of Proposed MIMO Antenna Systems

The proposed antenna is modelling based on the dimension of the single hexagon antenna which is presenting in Chapter Three. However, to approach a suitable prototype model, firstly, the size is chosen to be with a dimension of 20×14 mm^2; as shown in Figure 4.1. It is composed primarily of the top, substrate, and bottom layers. The top layer consists primarily of two parts; the first one is called a patch with multiple hexagonal concentric rings radiator geometric shapes. The second one is called a microstrip feed line with 50 Ω connected to the power source through an SMA connector. This layer is printed on an FR-4 substrate having 4.3 permittivity, 0.035 loss tangent, and a substrate thickness of 1.6 mm, representing the dielectric layer. The last layer is called the bottom or ground plane. It takes a partial ground plane form; it plays a crucial role in improving design bandwidth.

4.3 MIMO Antenna Model

To achieve a MIMO prototype, four elements of a single antenna are arranged in orthogonal directions to obtain the proposed antenna. The four congruent antenna elements are integrated onto a PCB, consisting of three layers of the patch, ground, and dielectric substrate. The same materials are used for a proposed single element with a square dimension of $38 \times 38 \times 1.6$ mm^3 shown in Figure 4.1.
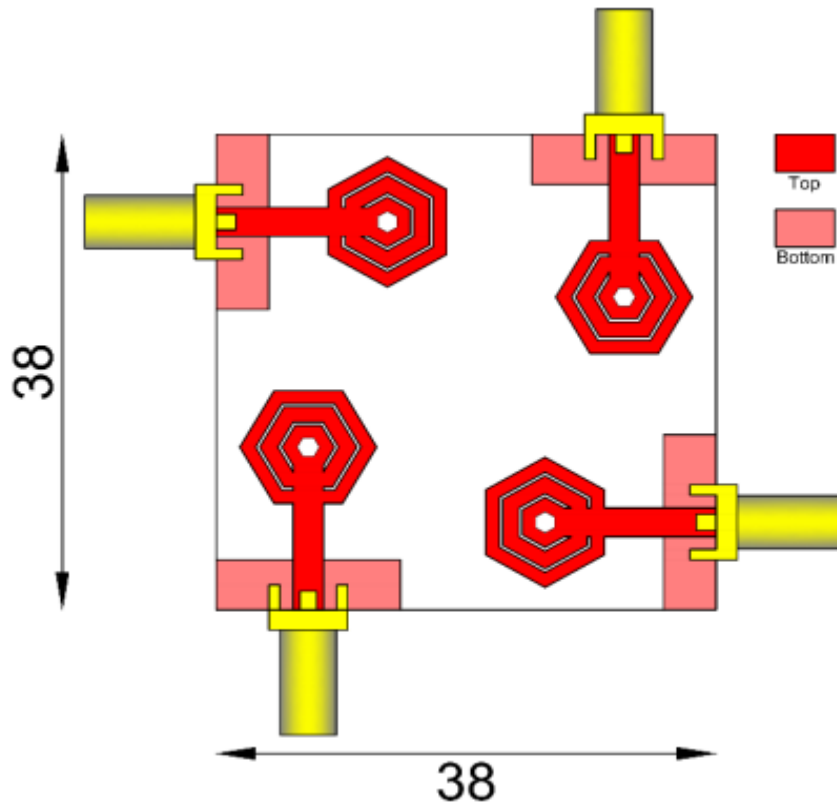
Figure 4. 1 The Geometry of the Proposed Dual-band MIMO Antenna.

4.4 Characteristics of MIMO Hexagon Antenna

In this section the characteristic MIMO Hexagon Antenna is presenting. Let us now depict the characteristics of the suggested antenna with optimal parameter values:

4.4.1 Gain of the Antenna

The gain across frequencies for the proposed MIMO hexagon antenna patch antenna is shown in Fig. 4-2. The curve clearly shows that the highest gain, equivalent to 4.4 dB, can be achieved at 7.5 GHz, while the lowest gain, equal to (1.5 dB), can be achieved at 3.05 GHz.
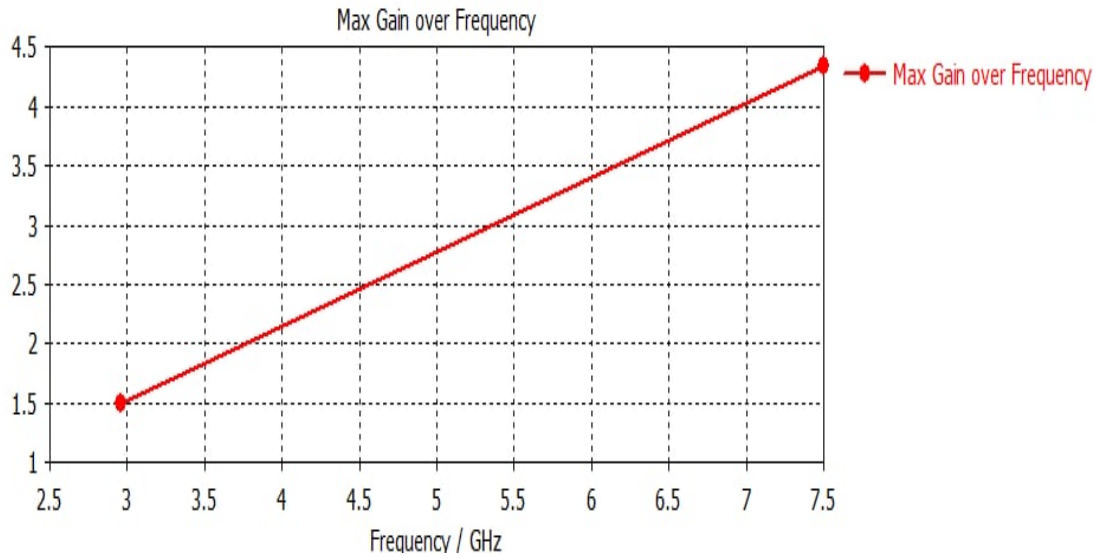
Figure 4. 2 Maximum Gain over Frequencies for the Proposed MIMO Hexagon
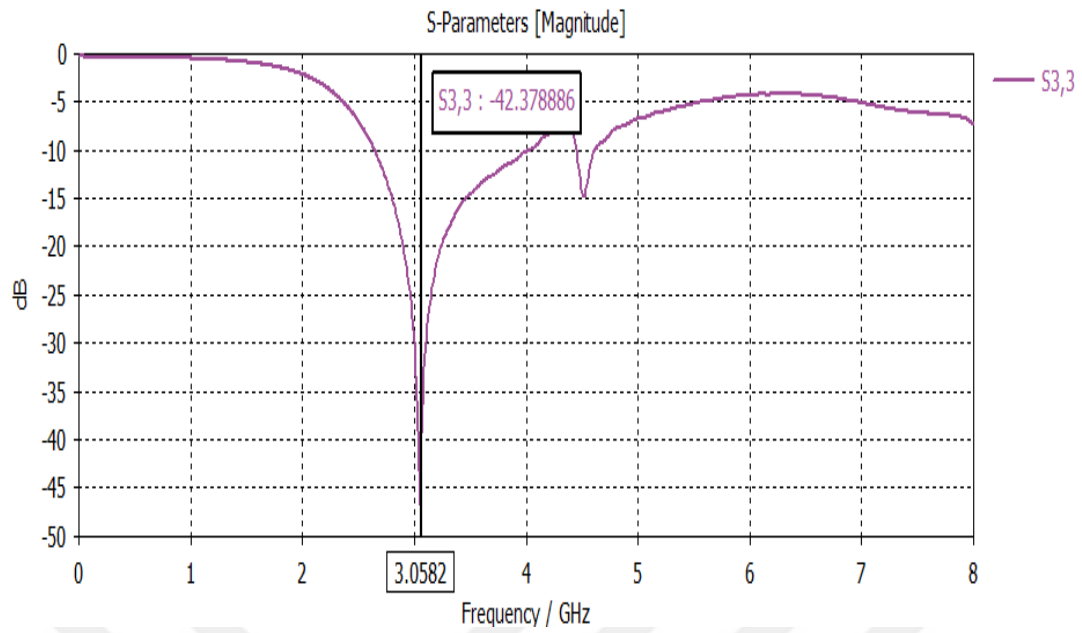Antenna.

4.4.2 S-parameter

The coefficient reflection or S-parameter of the proposed MIMO hexagon antenna
verses different frequencies values is presenting in Fig. 4.3. The extracting results for
the four antennas are achieved high coefficient reflection value close to the ideal value.
According to Fig. 4.3, the suggested MIMO Hexagon antenna attained a center
frequency of 3.05 GHz for all four antennas (a, b, c and d). Applications like Wi-Fi and
WiMAX are covered by this frequency. According to Figure 4.3.a, the first port of the
proposed MIMO Hexagon antenna S-parameter, Figure 4.3.b, the second port of the
proposed MIMO Hexagon antenna S-parameter, Figure 4.3.c, the third port of the
proposed MIMO Hexagon antenna S-parameter, and Figure 4.3.d, the fourth port, are
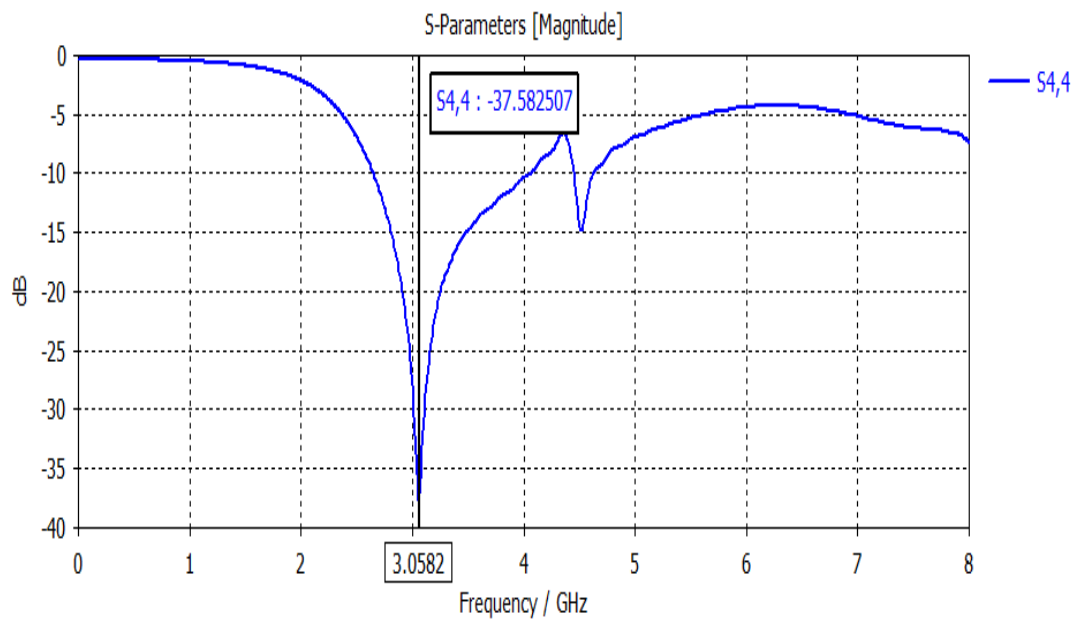each shown.
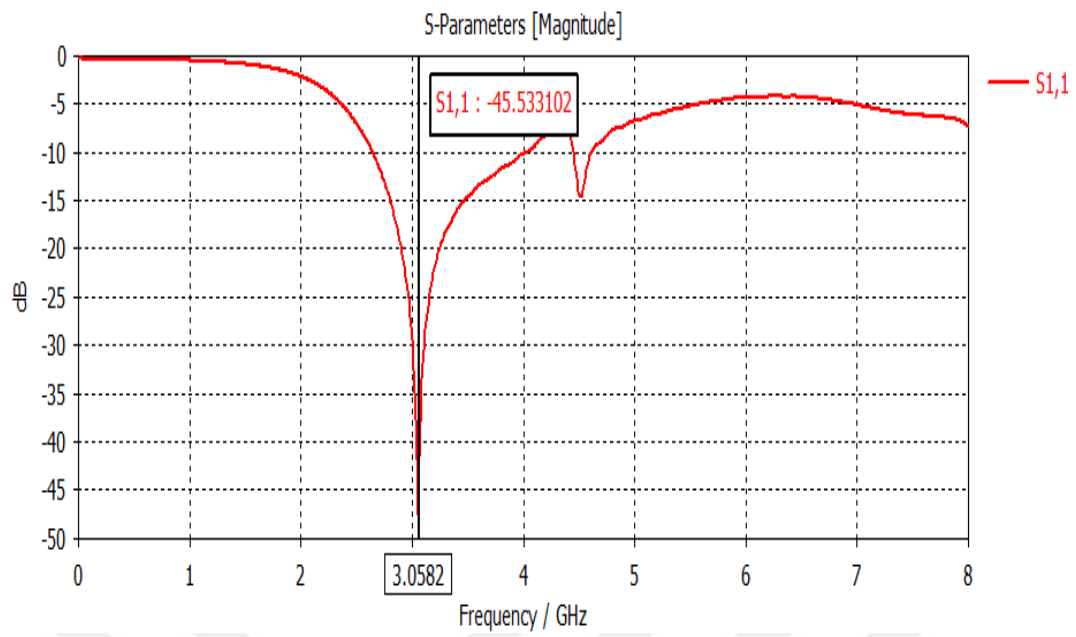
(a)
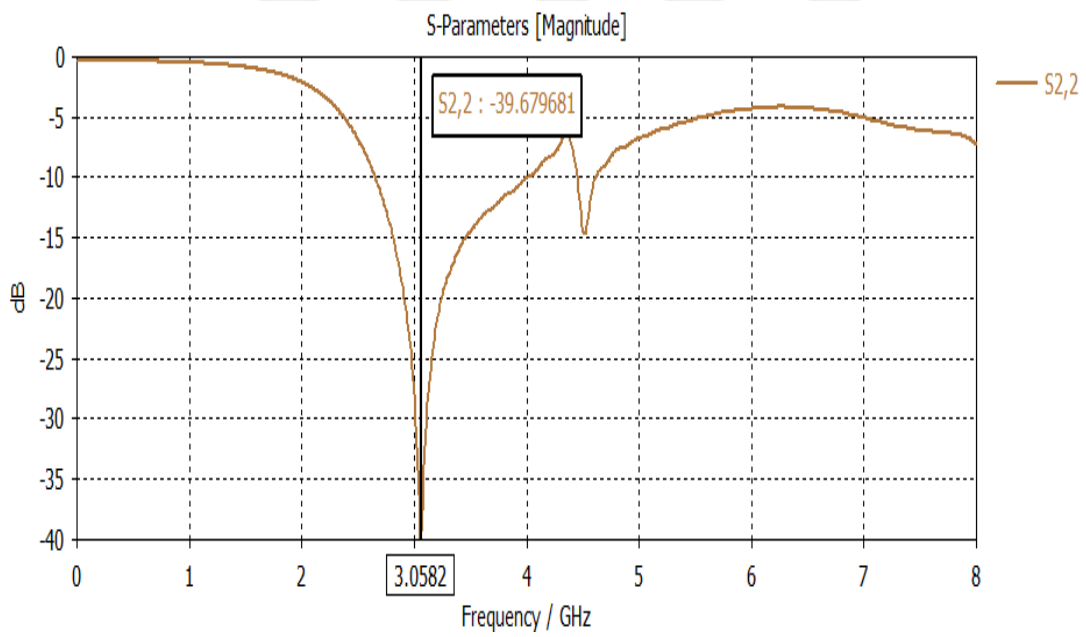
(b)

(c)

(d)

**Figure 4. 1** S-parameters for the Proposed MIMO Hexagon Antenna

4.4.3 Reference Impedance

In term of reference impedance, the proposed MIMO hexagon antenna have been tested to identified the value of reference impedance for different frequencies values. Where it is found that the value of the reference is close to 57 ohm. The reference impedance

considered very close to the ideal value of 50 ohm. However, the reference impedance the proposed MIMO Hexagon antenna shown in Fig. 4.4 (a, b, c and d). Fig. 4.4.a represent the first port of the proposed MIMO Hexagon antenna reference impedance, Fig. 4.4.b represent the second port of the proposed MIMO Hexagon antenna reference impedance, Fig. 4.4.c represent the third port of the proposed MIMO Hexagon antenna reference impedance, and Fig. 4.4.d represent the fourth port of the proposed MIMO Hexagon antenna reference impedance respectively.
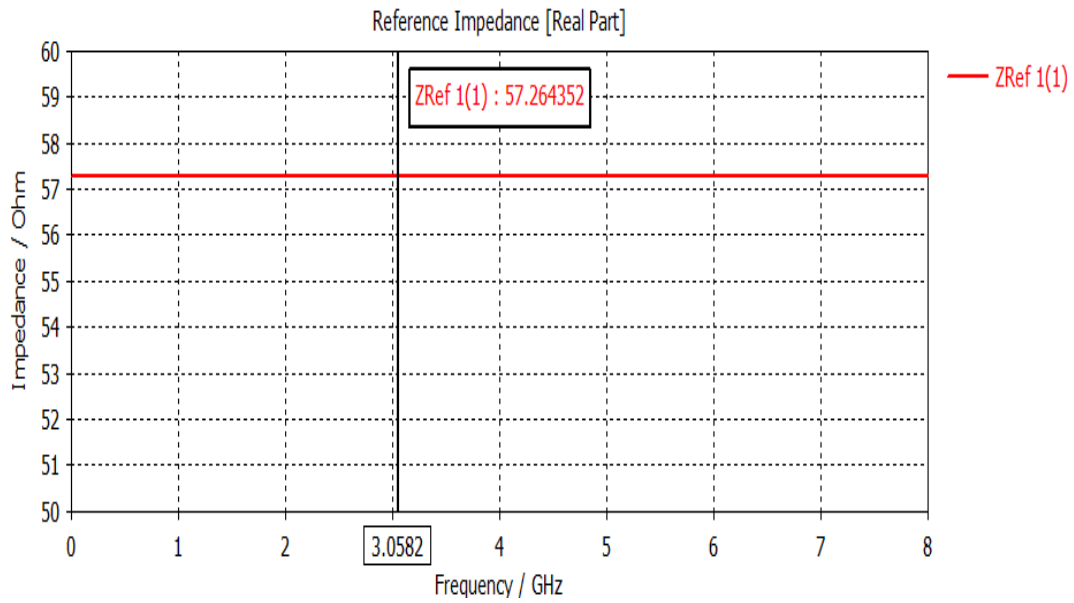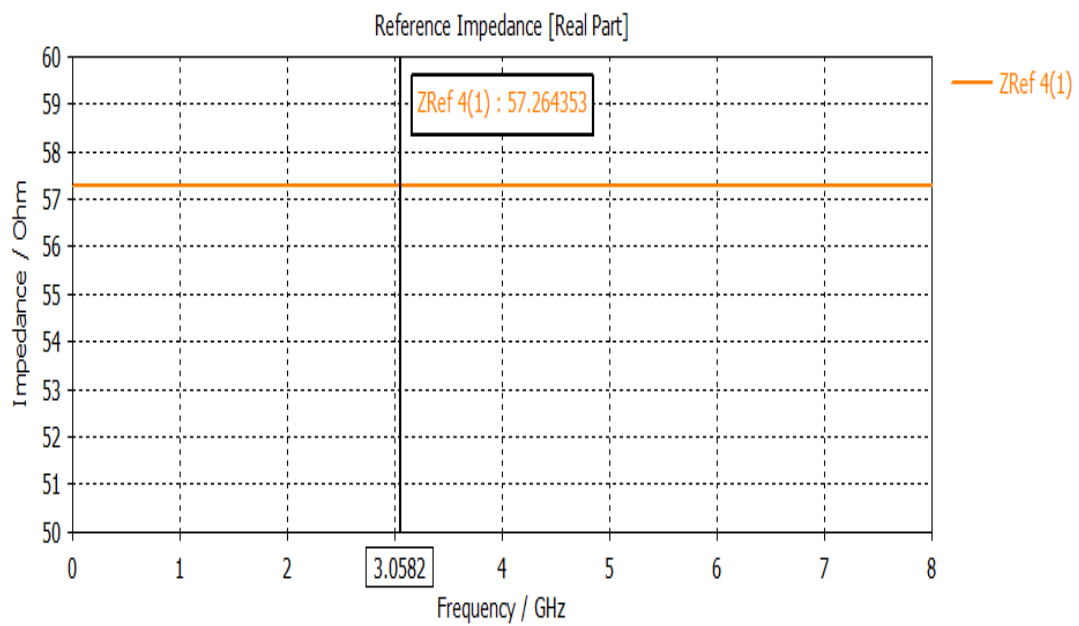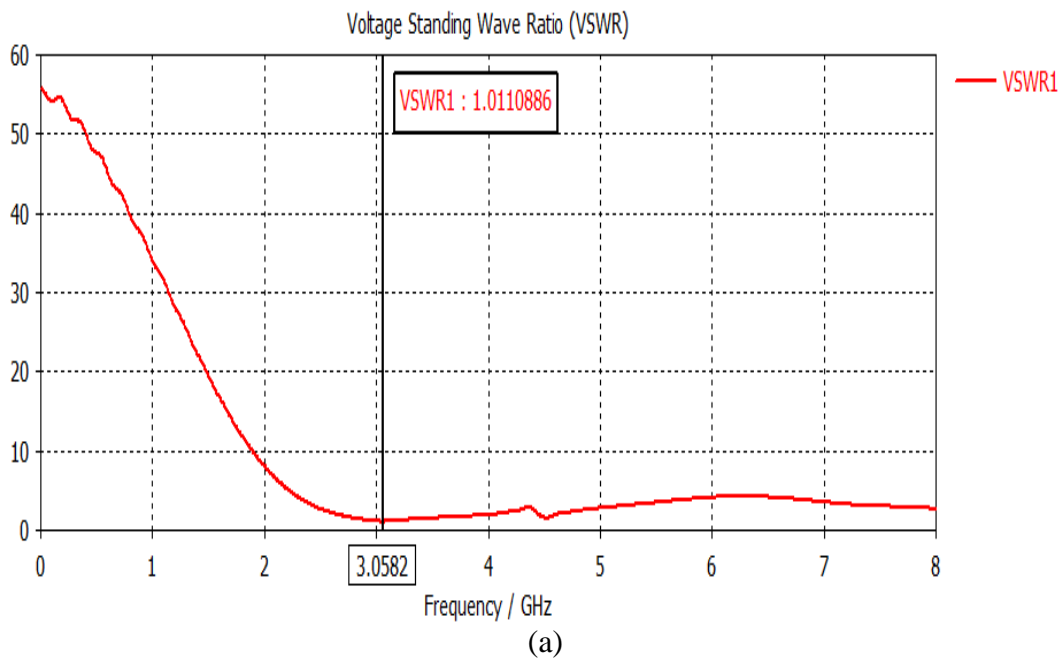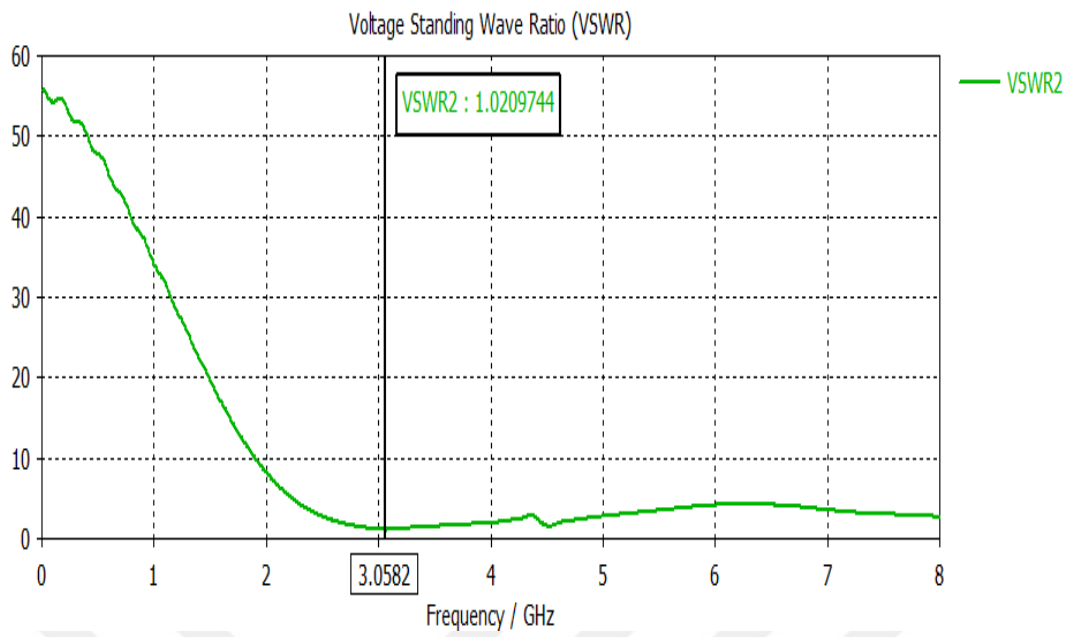

(a)
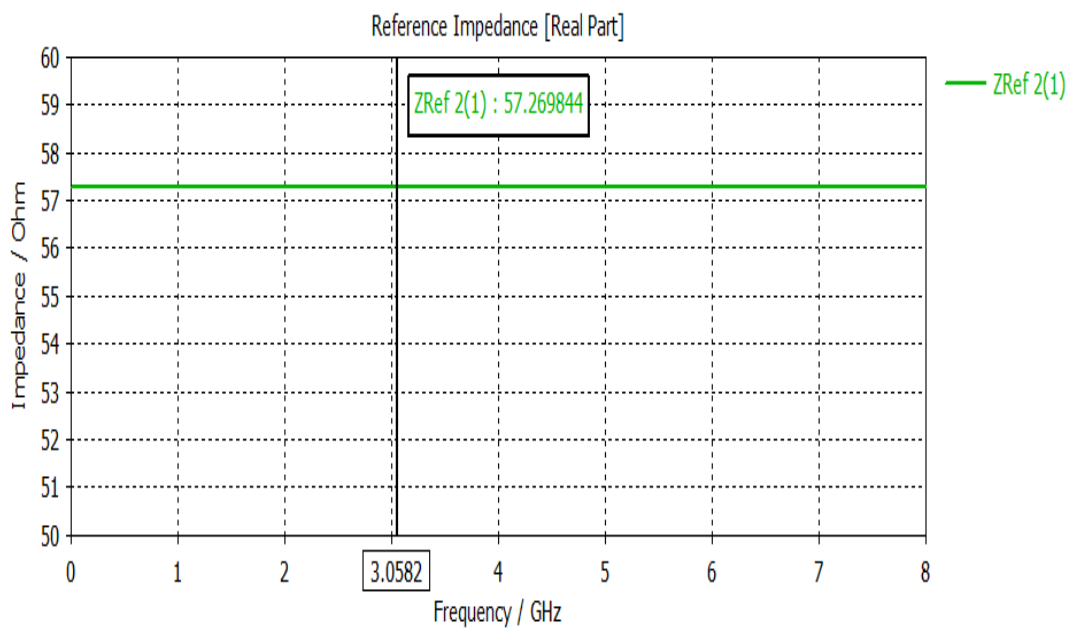
(b)
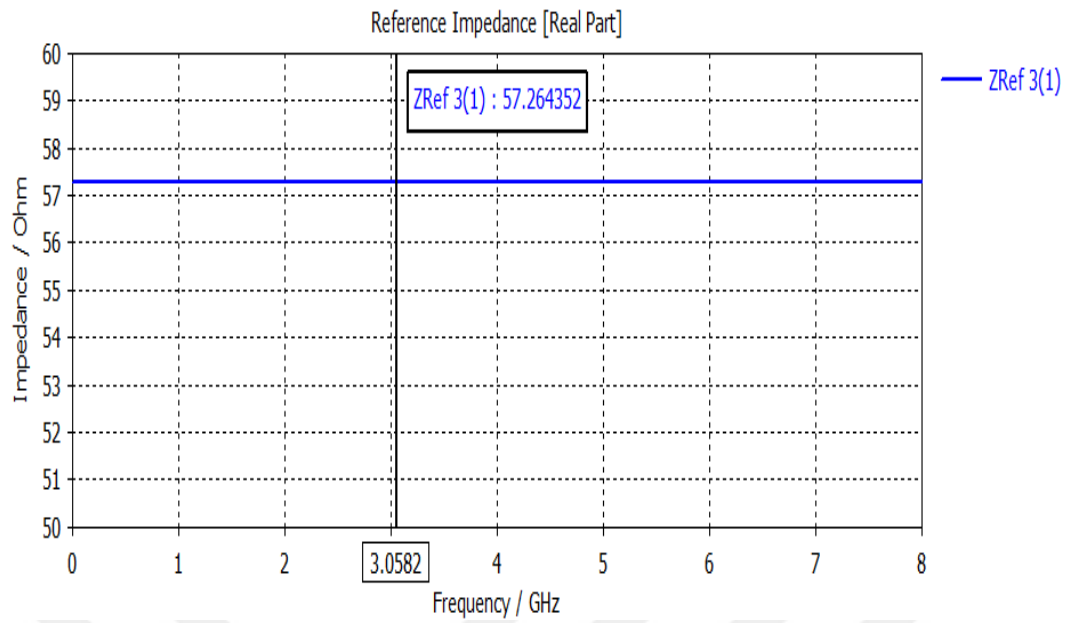
(c)

(d)

Figure 4. 2 Reference Variation for Different Frequency Value of the Proposed MIMO
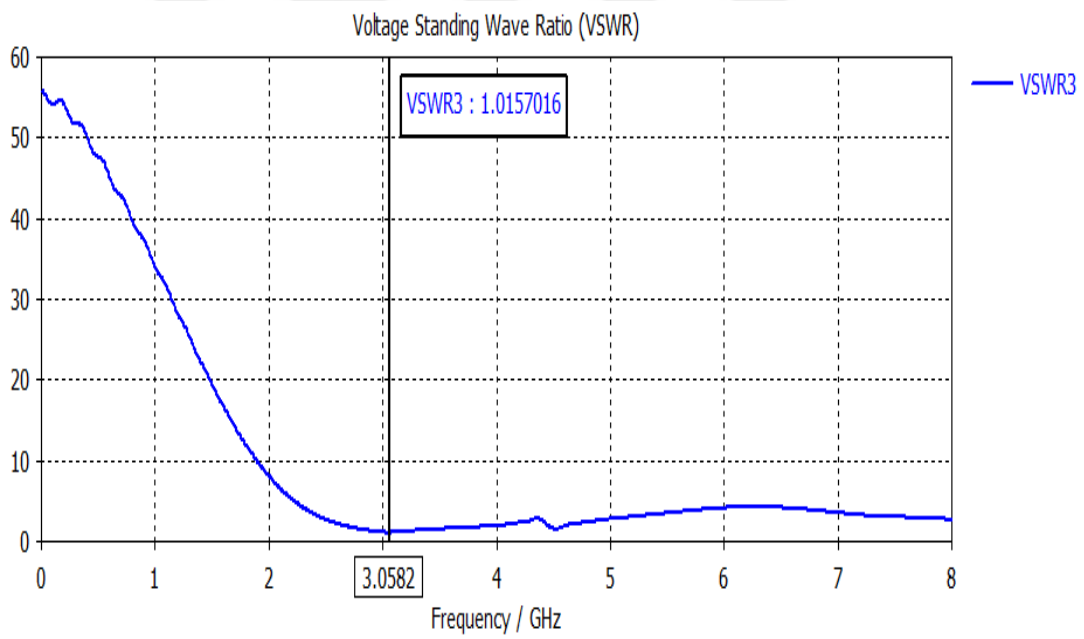Hexagon Antenna

4.4.4 Voltage Standing Wave Ratio

The proposed MIMO hexagon antenna's tested voltage standing wave ratio (VSWR) for a variety of frequencies is shown in Fig. 4.5. However, the suggested antenna's best VSWR results came in at 1.009. It is easy to see that the suggested antenna can perform well across a variety of frequency ranges. Figure 4.5.a shows the first port of the proposed MIMO Hexagon antenna VSWR, Figure 4.5.b shows the second port of the proposed MIMO Hexagon antenna VSWR, Figure 4.5.c shows the third port of the proposed MIMO Hexagon antenna VSWR, and Figure 4.5.d shows the fourth port, respectively.
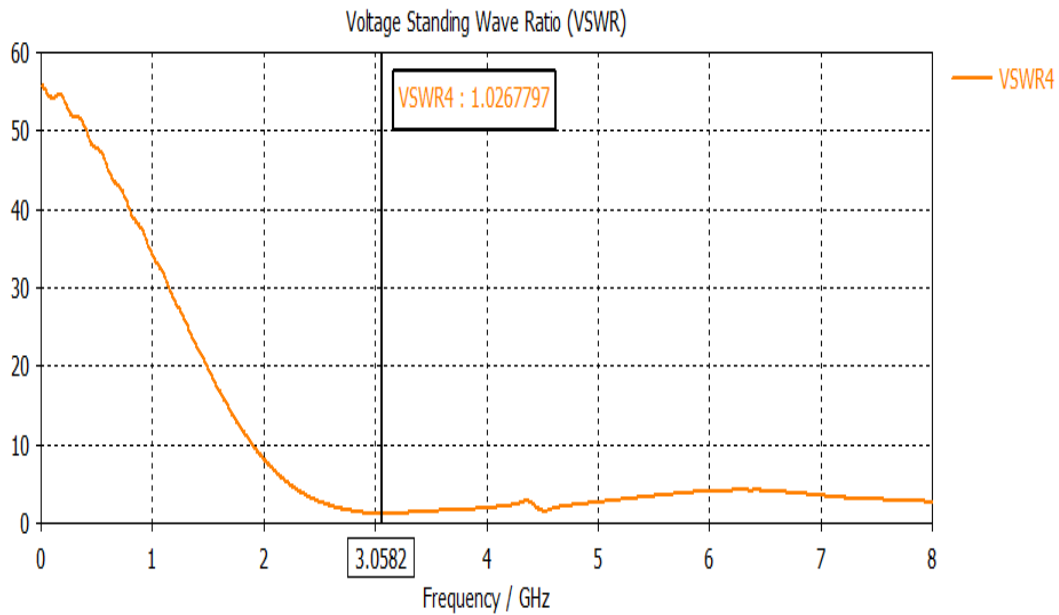

(a)

Voltage Standing Wave Ratio (VSWR)

VSWR2 : 1.0209744

Frequency / GHz

3.0582

VSWR2

(b)

Voltage Standing Wave Ratio (VSWR)

VSWR3 : 1.0157016
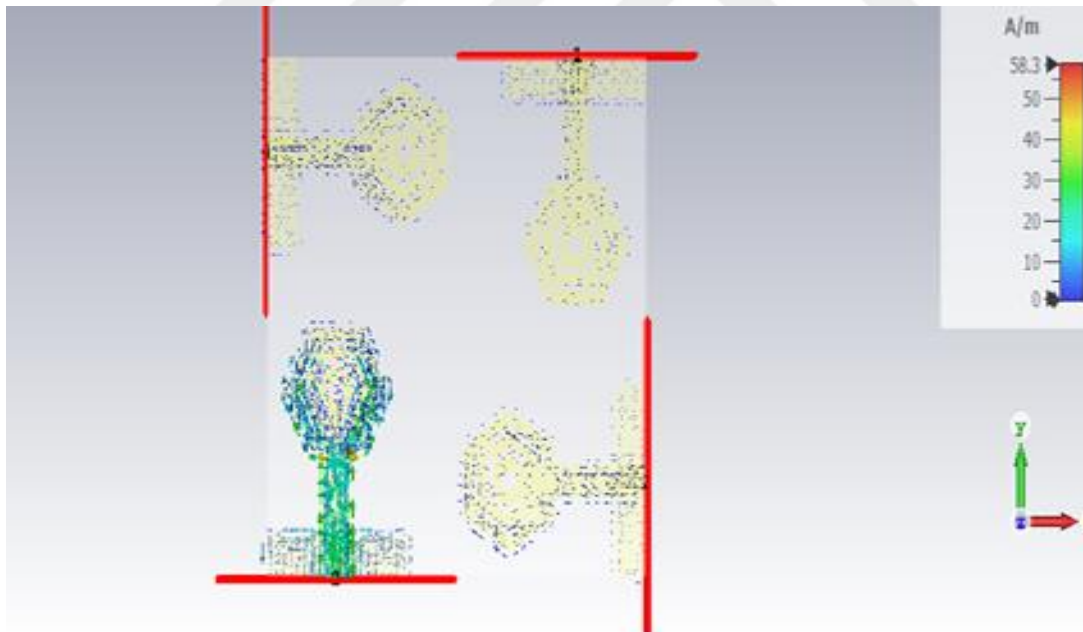
Frequency / GHz

3.0582

VSWR3

(c)

(d)

Figure 4. 3 VSWR Variation for Different Frequency Value of the Proposed MIMO
Hexagon Antenna

4.4.5 Current Distribution

In Fig. 4.6, the proposed MIMO hexagon antenna's current distributions at 3.36 GHz
are depicted. The first suggested MIMO Hexagon antenna, however, is shown in Figure
4.6(a) and it has a maximum current value of 57.8 A/m at the frequency of 3.05 GHz.
At a frequency of 3.05 GHz, the second port of the proposed MIMO Hexagon antenna
has a maximum current value of 58.3 A/m. The third port of the proposed MIMO
Hexagon antenna, which has a maximum current value of 57.8 A/m at the frequency of
3.05 GHz, is shown in Figure 4.6(c). The fourth port of the proposed MIMO Hexagon
antenna is shown in Fig. 4.6(d). It has a maximum current value of 57.2 A/m at 3.36
GHz.

(a)

(b)

49
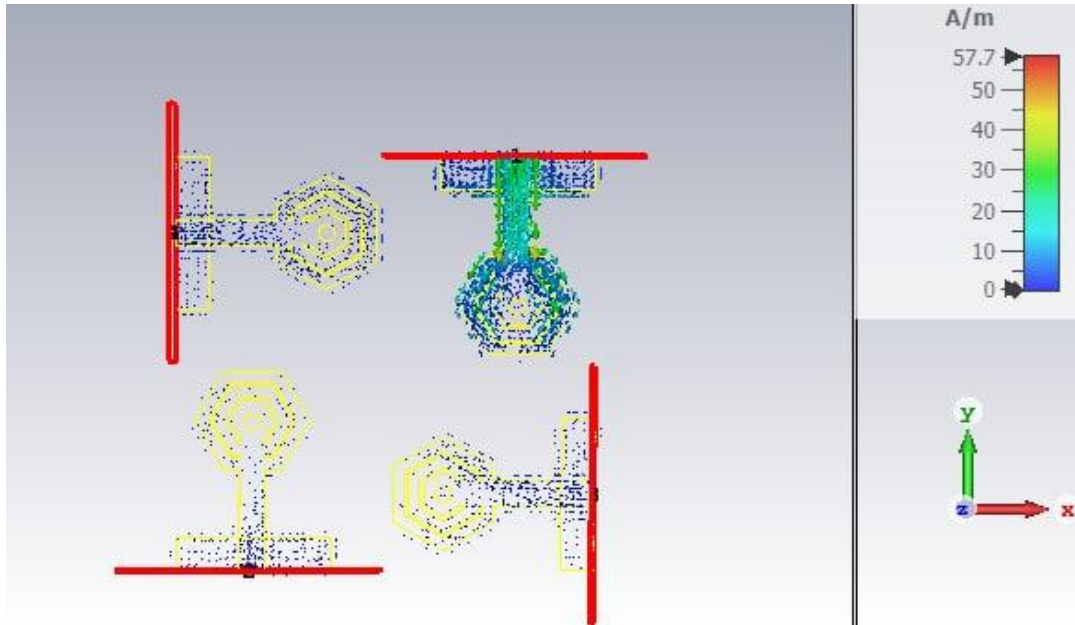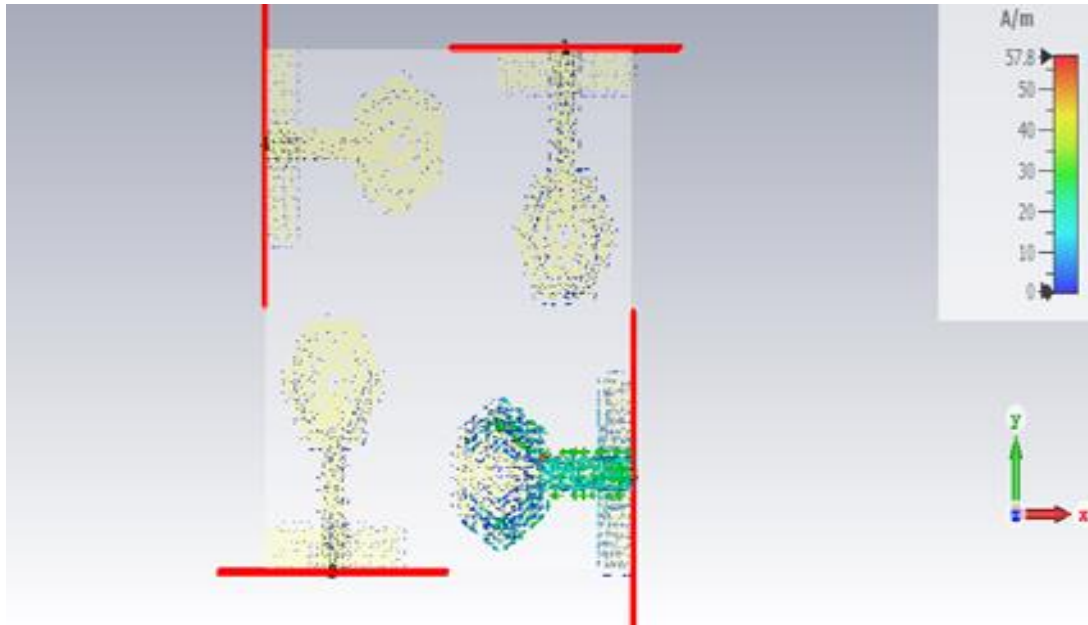
(c)

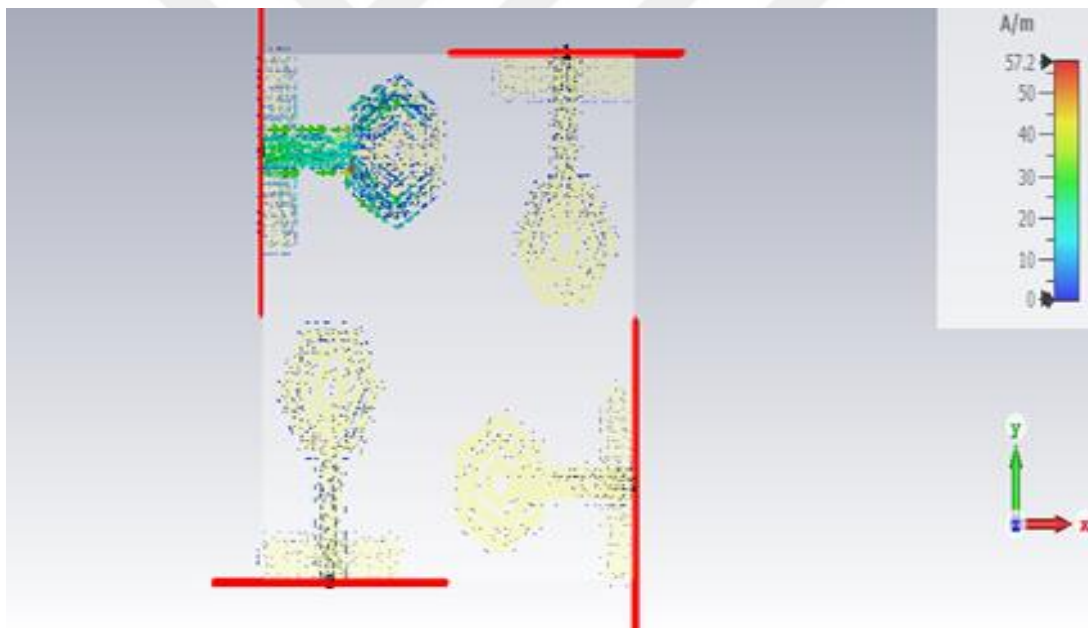

(d)

Figure 4. 6 Current Distributions of the Proposed MIMO Hexagon Antenna at 3.05 GHz for Different Ports.

4.4.6 Radiation Pattern

The radiation pattern of the proposed MIMO hexagon antenna is shown in Fig. 4.7 at central frequency of 3.05 GHz. It is clearly to observed that the radiation pattern at 3.36 GHz has a maximum directivity of 3.61 dB for the first port of the proposed antenna as shown in Fig.4.7.(a). Fig. 4.7.(b) represent the maximum directivity of 3.64 dB for the second port of the proposed antenna. Fig. 4.7.(c) represent the maximum directivity of 3.69 dB for the third port of the proposed antenna. Fig. 4.7.(d) represent the maximum directivity of 3.69 dB for the fourth port of the proposed antenna. It is pure to see that these designs, in general, have qualities that attain bandwidth, which is necessary for a wide variety of applications.
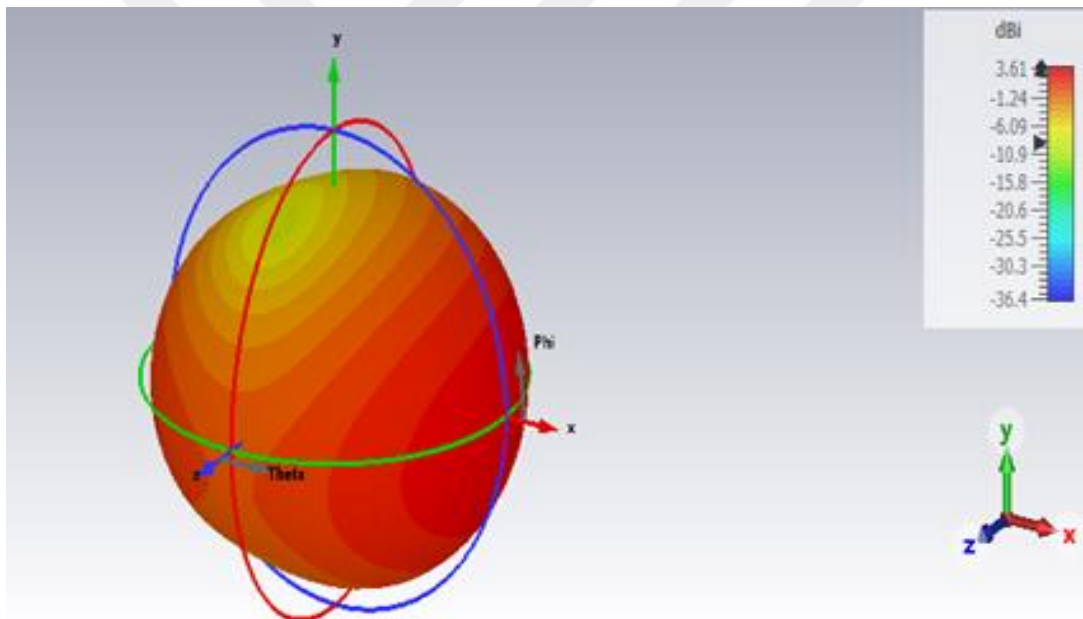
(a)
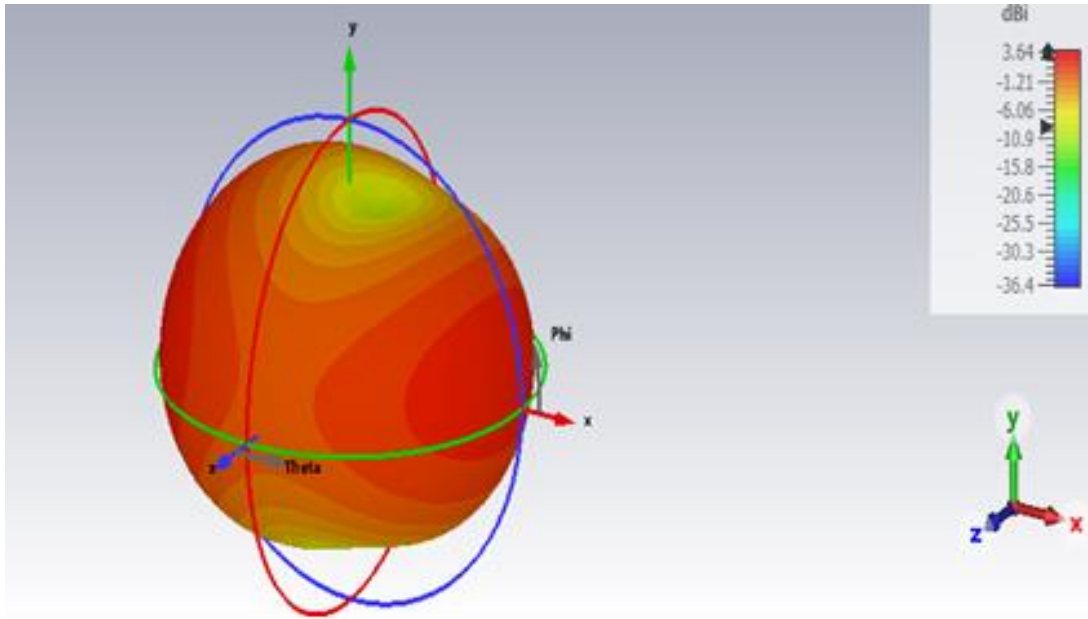
(b)

(C)

(d)

Figure 4. 4 Radiation Pattern of the Proposed MIMO Hexagon Antenna

at 3.05 GHz for Different Ports.

4.4.7 Current Density

The current density of the proposed MIMO hexagon antenna is shown in Fig. 4.8 at central frequency of 3.05 GHz. It is clearly to observed that the current density at 3.05 GHz has a maximum current of 208 A/m^2 for the first port of the proposed antenna as shown in Fig.4.8.(a). Fig. 4.8.(b) represent the maximum current density of 212 A/m^2 for the second port of the proposed antenna. Fig. 4.7.(c) represent the maximum current density of 209 A/m^2 for the third port of the proposed antenna. Fig. 4.8.(d) represent the maximum current density of 206 A/m^2 for the fourth port of the proposed antenna. It is pure to 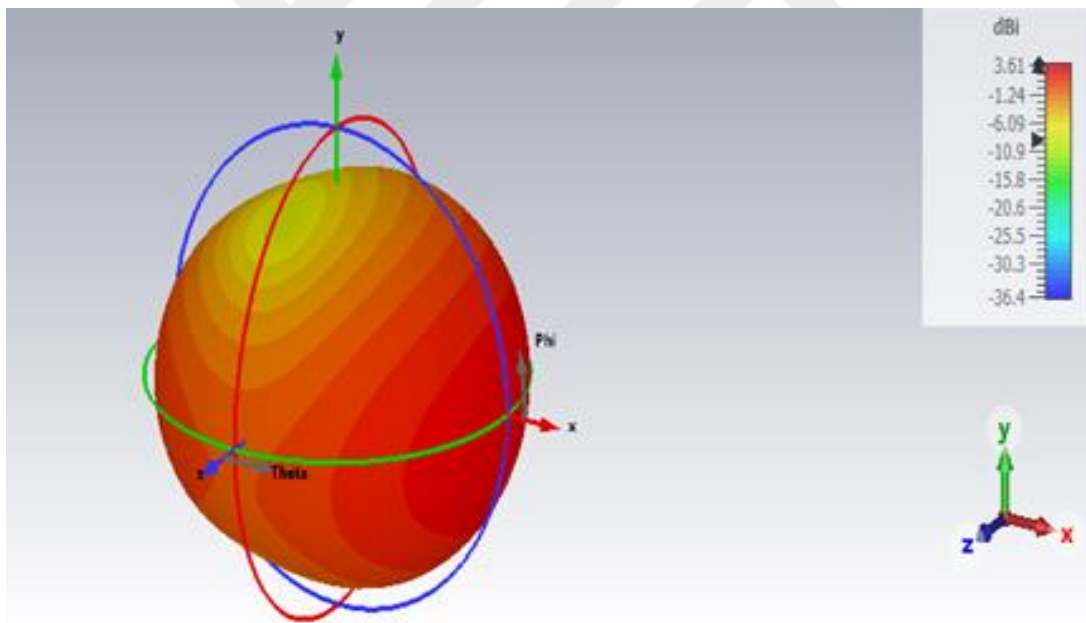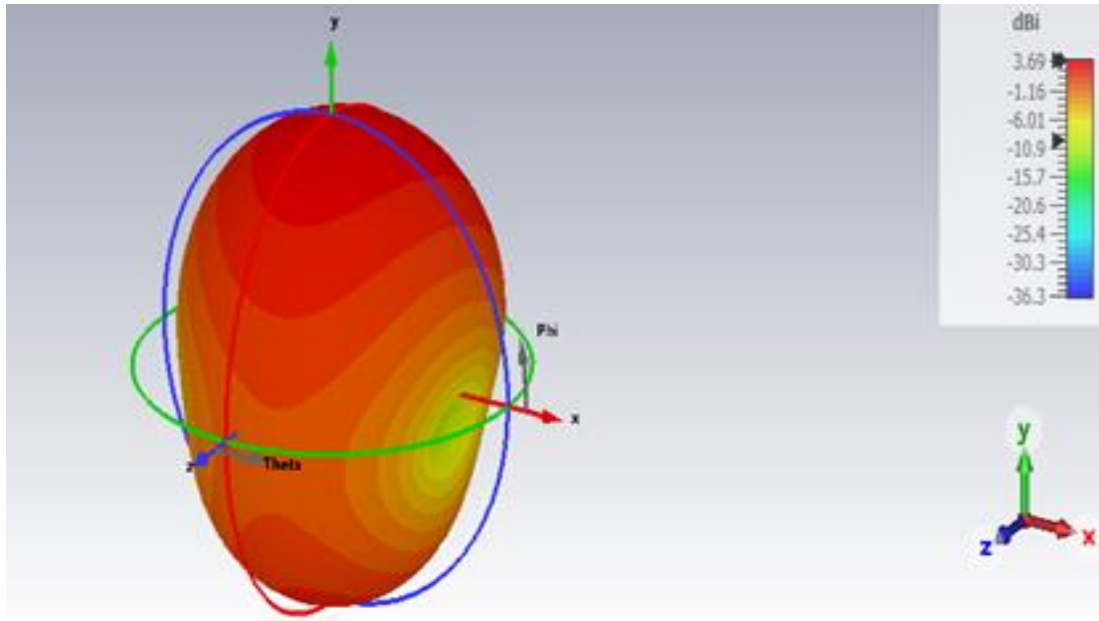see that propose design have maximum current density that m The current density of the proposed MIMO hexagon antenna is shown in Fig. 4.8 at central frequency of 3.05 GHz. It is clearly to observed that the current density at 3.05 GHz has a maximum current of 208 A/m2 for the first port of the proposed antenna as shown in Fig.4.8.(a). Fig. 4.8.(b) represent the maximum current density of 212 A/m2 for the second port of the proposed antenna. Fig. 4.7.(c) represent the maximum current density of 209 A/m2 for the third port of the proposed antenna. Fig. 4.8.(d) represent the

maximum current density of 206 A/m2 for the fourth port of the proposed antenna. It is pure to see that propose design have maximum current density that make it as competitive antenna for the application of both Wi-Fi and make it as competitive antenna for the application of both Wi-Fi and WiMAX.
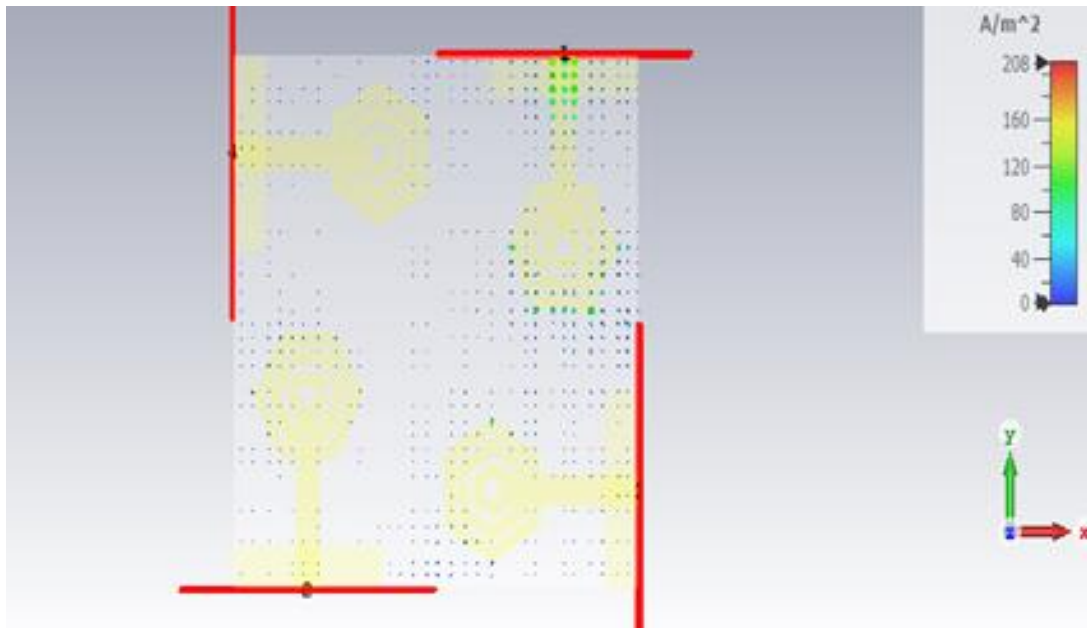
(a)

(b)
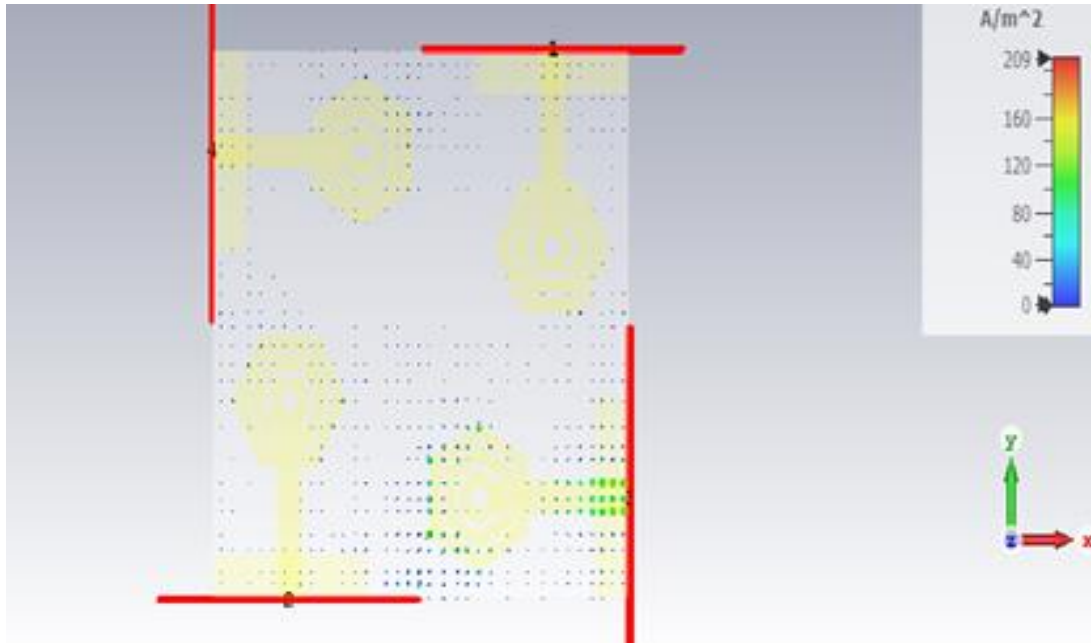
(c)

(d)

Figure 4. 8 Current Density of the Proposed MIMO Hexagon Antenna
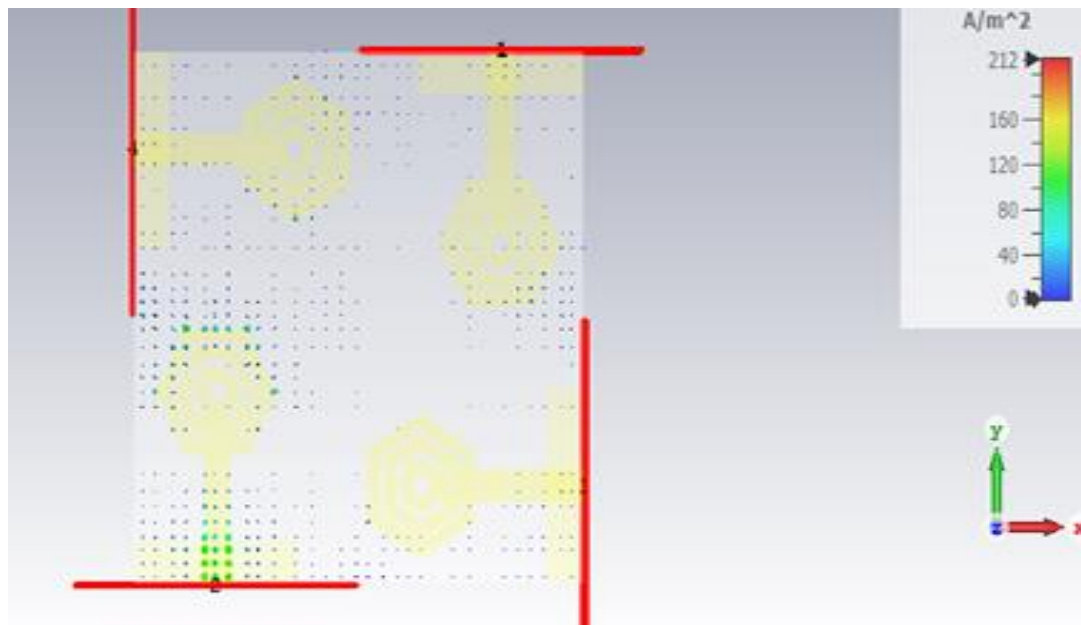
at 3.05 GHz for Different Ports.

4.4.8 Energy Density

The energy density of the proposed MIMO hexagon antenna is shown in Fig. 4.9 at central frequency of 3.05 GHz. It is clearly to observed that the current density at 3.36 GHz has a maximum energy density of 1.2×10^{-3} j/m^3 for the first port of the proposed antenna as shown in Fig.4.9. (a). Fig. 4.9.(b) represent the maximum energy density of 1.2×10^{-3} j/m^3 for the second port of the proposed antenna. Fig. 4.7.(c) represent the maximum energy density of 1.2×10^{-3} j/m^3 for the third port of the proposed antenna. Fig. 4.9.(d) represent the maximum energy density of 1.2×10^{-3} j/m^3 for the fourth port of the proposed antenna.
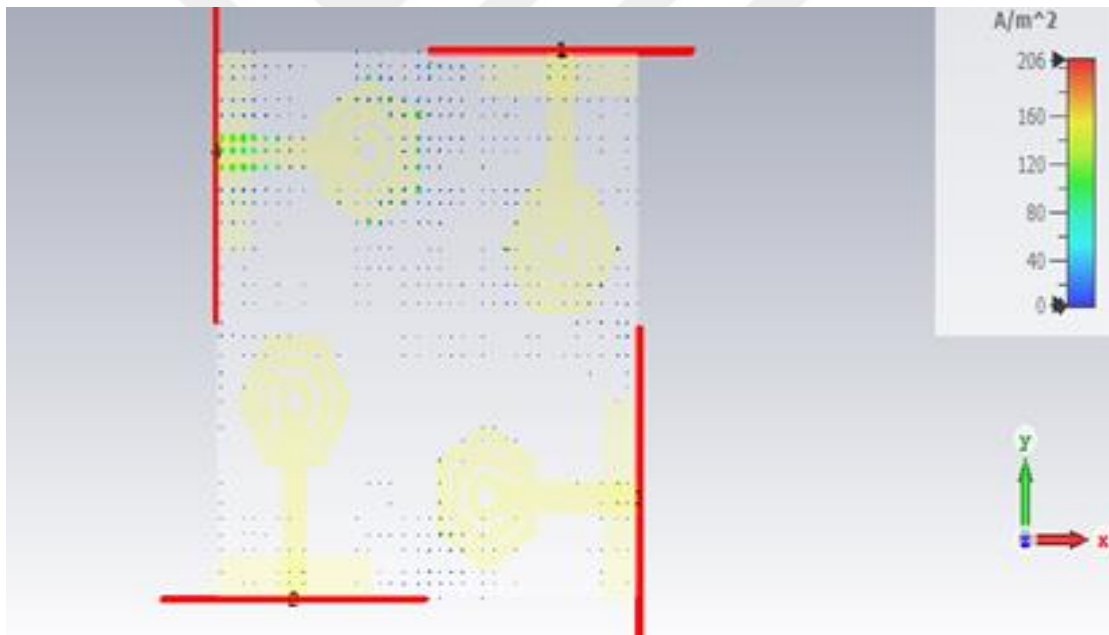

(a)

(b)

(c)

57
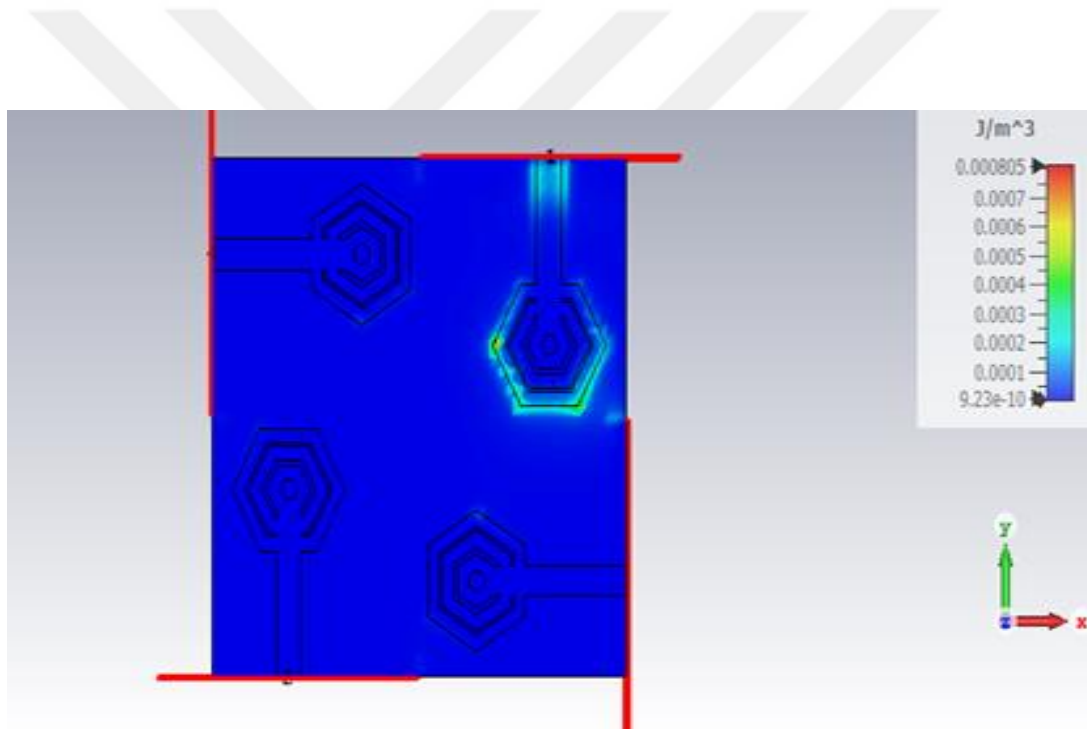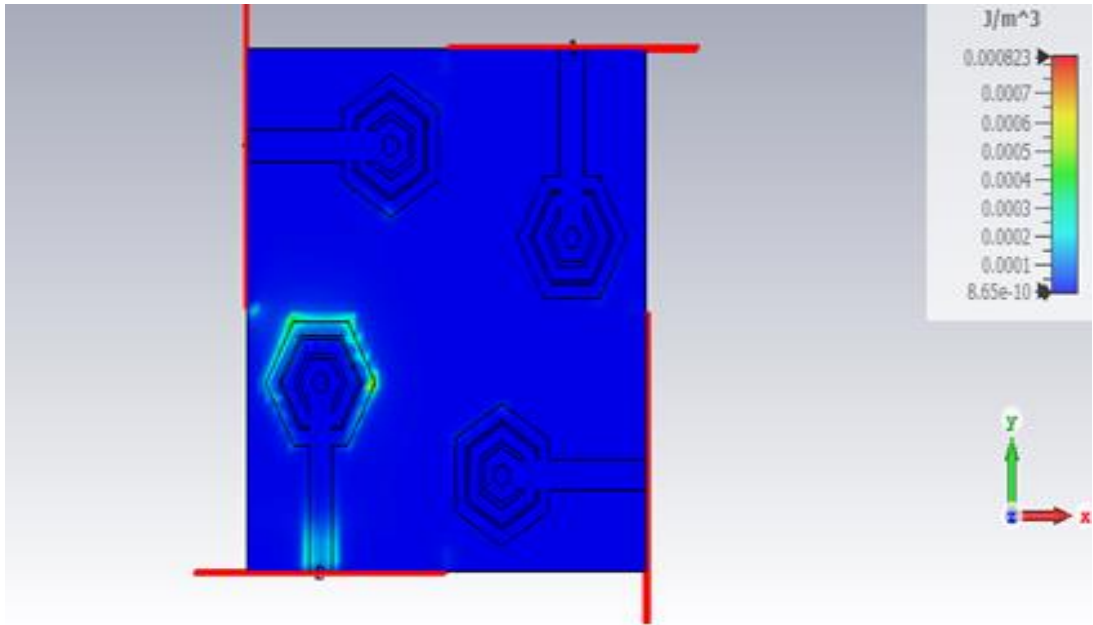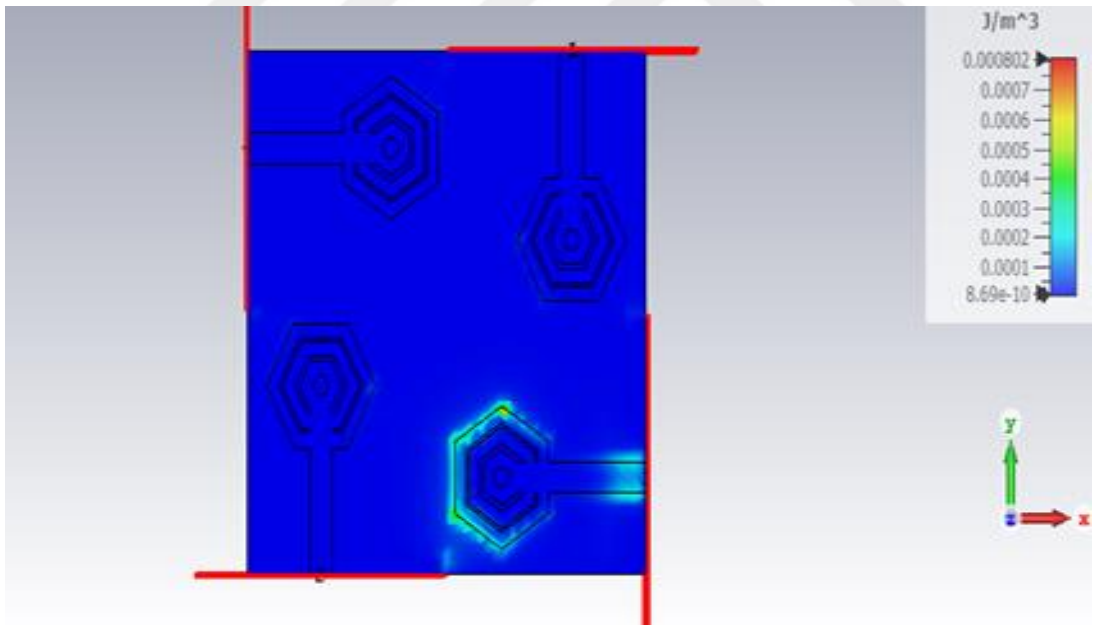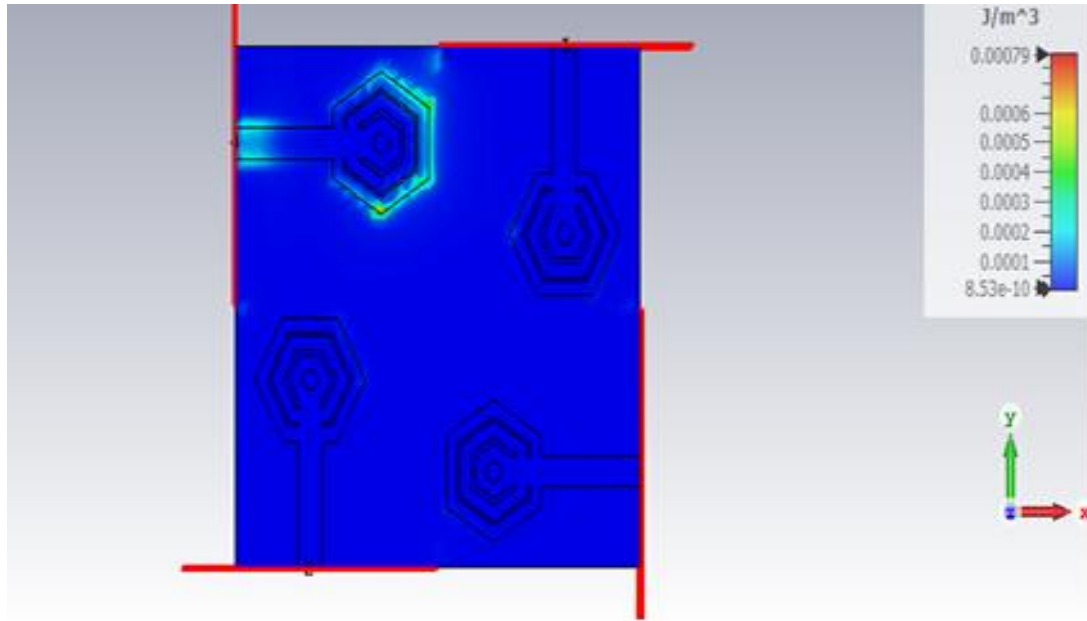
(d)

Figure 4. 9 Energy Density of the Proposed MIMO Hexagon Antenna

at 3.05 GHz for Different Ports

4.4.9 Far filed Patterns

The Far filed radiation patterns of the proposed MIMO hexagon antenna is shown in Fig.4.10. The results of the radiation patterns for both main lob magnitude, main lob direction, angular width is presenting, and side lob level. Fig. 4.10.(a) represent the first port of the proposed MIMO Hexagon antenna Far filed radiation patterns with main lob magnitude of 0.835 dBi, main lob direction of 171-degree, angular width of 99.5 degree and side lob level of -0.9 dB. Fig. 4.10.(b) represent the second port of the proposed MIMO Hexagon antenna Far filed radiation patterns with main lob magnitude of 0.787 dBi, main lob direction of 172-degree, angular width of 101.6 degree and side lob level of -1 dB. Fig. 4.10.(c) represent the third port of the proposed MIMO Hexagon antenna Far filed radiation patterns with main lob magnitude of 3.66 dBi, main lob direction of 105-degree, angular width of 157.4 degree and side lob level of -1.9 dB. Fig. 4.10.(d) represent the fourth port of the proposed MIMO Hexagon antenna Far filed radiation patterns with main lob magnitude of 3.66 dBi, main lob direction of 106-degree, angular width of 157.9 degree and side lob level of -1.9 dB.

Farfield Directivity Abs (Phi=90)

—— farfield (f=2.955) [1]

Phi= 90   0   Phi=270
              30   30
         60   60

    90   90
              -8 -6 -4 -2 0

        120   120

              150   150
                   180

Theta / Degree vs. dBi
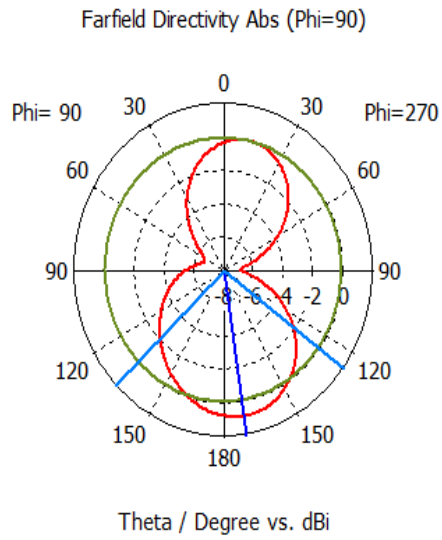
Frequency = 2.955 GHz
Main lobe magnitude =   0.835 dBi
Main lobe direction = 171.0 deg.
Angular width (3 dB) =   99.5 deg.
Side lobe level =   -0.9 dB

(a)

Farfield Directivity Abs (Phi=90)

—— farfield (f=2.955) [2]

Phi= 90   0   Phi=270
              30   30
         60   60

    90   90
              -8 -6 -4 -2 0

        120   120

              150   150
                   180

Theta / Degree vs. dBi
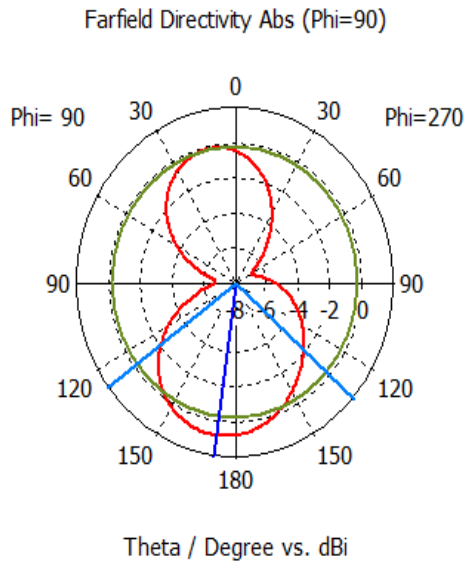
Frequency = 2.955 GHz
Main lobe magnitude =   0.787 dBi
Main lobe direction = 172.0 deg.
Angular width (3 dB) = 101.6 deg.
Side lobe level =   -1.0 dB

(b)

59

Farfield Directivity Abs (Phi=90)

— farfield (f=2.955) [3]

Frequency = 2.955 GHz
Main lobe magnitude =   3.66 dBi
Main lobe direction = 105.0 deg.
Angular width (3 dB) = 157.4 deg.
Side lobe level =   -1.9 dB

Theta / Degree vs. dBi

(c)

Farfield Directivity Abs (Phi=90)
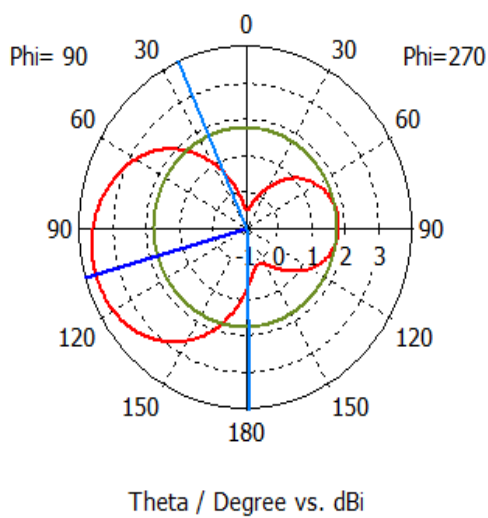
— farfield (f=2.955) [4]

Frequency = 2.955 GHz
Main lobe magnitude =   3.66 dBi
Main lobe direction = 106.0 deg.
Angular width (3 dB) = 157.9 deg.
Side lobe level =   -1.9 dB

Theta / Degree vs. dBi

(d)

Figure 4. 10 Far Field Pattern of the Proposed MIMO Hexagon Antenna
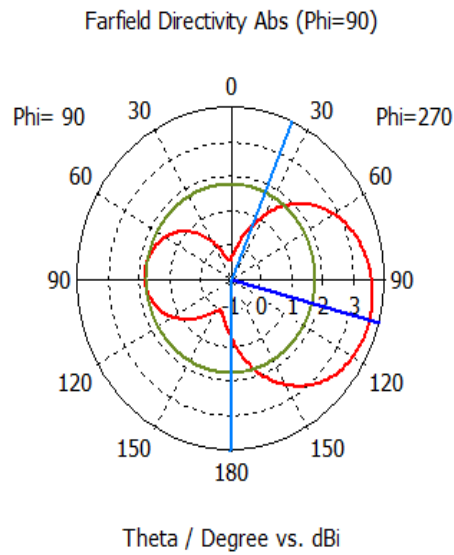
at 3.05 GHz for Different Ports

4.5 . Design comparison

In this section, the proposed antenna (the MIMO hexagon antenna) is compared with previous antenna designs in terms of Size, Gain and Bandwidth. The comparison is presented based on recent antenna designs, as shown in the Table 4.1. The proposed antenna can be considered as new competitive antenna for future 5G application based on its size reduction, wide bandwidth, and gains. As presenting in the Table 4.1 the propose antenna has bandwidth of 1.2 GHz with gain of 3.5.

Table 4.1. Comparative Chart.

Reference	Size (mm)	Antenna Type	Operating Frequency	Gain	Bandwidth (GHz)
(Chang, et al. 2021)	71×71×4	MIMO	2.38~2.53 GHz, 3.29~4.11 GHz, and 4.72~5.01	4	0.15 0..82 0.29
(Molins-Benlliure, et al, 2022)	108 ×43.8 ×34.2	MIMO	4 GHz	-10	4.8
(Han, Xiao, Chen, & Yuan, 2020)	76×150×7	MIMO	4.71 GHz	6.2	0.2
(Ji.Z et al., 2021)	120.5 ×130 ×0.8	MIMO	3.55 GHz	6.4	0.5
(Sun, et al, 2019)	40×40×7.5	MIMO	3.65 GHz	-	1.2
(Li, et al, 2020)	32×32×1.47	Single	3.4 GHz	6.4	0.5
Proposed antenna	38×38×1.6	MIMO	3.05 GHz	3.5	1.2

CHAPTER FIVE

CONCLUSIONS AND SUGGESTIONS FOR FUTURE WORKS

5.1. Conclusions

Two antennas have been proposed and created in this study that are practical for numerous wireless application needs. Excellent agreement between observed and simulated data, spanning the 3 to 10 GHz range, was found. These three antennas' findings demonstrate that it is practical for many UWB applications. The recommended designs provide a practical solution for the suitability of elliptical, circular, and rectangular patch antennas used in UWB applications. This research leads to the following conclusions:

1. These two antennas outperform certain other large-size designs, making them better suited for numerous significant wireless applications.
2. The bandwidth, current distribution, gain, impedance, and radiation pattern of an antenna array are significantly influenced by the geometry of the ground in the array.
3. Extensive research was done in the hexagon antenna to extract the time-domain behavior of the notch frequency antenna. Despite the notch appearing in the frequency domain, it appears that there is little distortion in the sent and received signal, making it suitable for use as a UWB antenna.
4. It can be seen from the rectangular patch antenna findings that a substantial bandwidth between 3.1 GHz and 10 GHz has been obtained for the recommended antenna that might be used in ultra-wideband communication systems.

5.2. "Suggestions for Future Works"

The suggestions for upcoming development as follow:

1. Fractal geometry has a role in reducing the size of the planned antenna.

2. Another patch antenna form is created in order to maximize the bandwidth gained.

3. Increase the element count and alter the ground plane to increase bandwidth and gain.

4. These three antennas might have been enhanced to achieve better bandwidth with a smaller size that could make them an appropriate option for 4G and 5G mobile systems based on the acceptable results of these three antennas, which are connected to their small size.

REFERENCES

Agboje, O., Nkordeh, N., Idiake, U. S., Oladoyin, O., Okokpujie, K., & Bob-Manuel, I. J. T. (2020). MIMO channels: optimizing throughput and reducing outage by increasing multiplexing gain. *18*(1), 419-426.

Ahad, A., Tahir, M., Aman Sheikh, M., Ahmed, K. I., Mughees, A., & Numani, A. J. S. (2020). Technologies trend towards 5G network for smart health-care using IoT: A review. *20*(14), 4047.

Al-Ani, N. M. K., Al-Ani, O. A. S., Mosleh, M. F., & Abd-Alhameed, R. A. (2021). *A Dual-Polarized MIMO Array Antenna System for Future Smartphone.* Paper presented at the Journal of Physics: Conference Series.

Al-Ani, N. M. K., Al-Ani, O. A. S., Mosleh, M. F., AbdAlhameed, R. A. J. I. J. o. I. T., & Science, C. (2020). A Design of MIMO System Based on YShaped with QSCS for UWB Applications. *12*(1), 17-23.

Al-Ogaili, F., & Shubair, R. M. (2016). *Millimeter-wave mobile communications for 5G: Challenges and opportunities.* Paper presented at the 2016 IEEE International Symposium on Antennas and Propagation (APSURSI).

Ancans, G., Bobrovs, V., Ancans, A., & Kalibatiene, D. J. P. C. S. (2017). Spectrum considerations for 5G mobile communication systems. *104*, 509-516.

Assimonis, S. D., Yioultsis, T. V., Antonopoulos, C. S. J. I. T. o. A., & Propagation. (2012). Design and optimization of uniplanar EBG structures for low profile antenna applications and mutual coupling reduction. *60*(10), 4944-4949.

Azari, A. J. I. t. o. a., & propagation. (2011). A new super wideband fractal microstrip antenna. *59*(5), 1724-1727.

Balanis, C. A. (2015). *Antenna theory: analysis and design*: John wiley & sons.

Ban, Y.-L., Li, C., Wu, G., & Wong, K.-L. J. I. a. (2016). 4G/5G multiple antennas for future multi-mode smartphone applications. *4*, 2981-2988.

Benlliure, J. M.; Fabrés, M. C.; Daviu, E. A.; Bataller, M. F. Sector Unit-Cell Methodology for the Design of Sub-6 GHz 5G MIMO Antennas. *IEEE Access*, 2022, 10, 100824-100836.

Chang, L.; Zhang, G.; Wang, H. Triple-Band Microstrip Patch Antenna and its Four-Antenna Module Based on Half-Mode Patch for 5G 4 × 4 MIMO Operation. *IEEE Transactions on Antennas and Propagation*, 2022, 70, 67-74.

Chakraborty, S., Rahman, M. A., Hossain, M., Mobashsher, A. T., Nishiyama, E., & Toyoda, I. J. S. A. S. (2020). A 4-element MIMO antenna with orthogonal circular polarization for sub-6 GHz 5G cellular applications. *2*(7), 1-13.

Chakraborty, S., Rahman, M. A., Hossain, M. A., Mobashsher, A. T., Nishiyama, E., & Toyoda, I. (2019). *Design and performance studies of a MIMO antenna with circular polarization diversity for 5G applications.* Paper presented at the 2019 5th International Conference on Advances in Electrical Engineering (ICAEE).

Chataut, R., & Akl, R. J. S. (2020). Massive MIMO systems for 5G and beyond networks—overview, recent trends, challenges, and future research direction. *20*(10), 2753.

Dadgarpour, A., Zarghooni, B., Virdee, B. S., Denidni, T. A., Kishk, A. A. J. I. A., & Letters, W. P. (2016). Mutual coupling reduction in dielectric resonator antennas using metasurface shield for 60-GHz MIMO systems. *16*, 477-480.

Fan, Y. (2018). Circularly Polarized Two-Dimensional Microstrip Standing-Wave Array Antenna.

Gao, S. S., Luo, Q., & Zhu, F. (2014a). *Circularly polarized antennas*: John Wiley & Sons.

Gao, S. S., Luo, Q., & Zhu, F. (2014b). Introduction to circularly polarized antennas.

Garcia, J., Arriola, A., Casado, F., Chen, X., Sancho, J., Valderas, D. J. I. m., antennas, & propagation. (2012). Coverage and read range comparison of linearly and circularly polarised radio frequency identification ultra-high frequency tag antennas. *6*(9), 1070-1078.

Gupta, R. J. I. J. o. E. T., & Technology. (2015). A comparative study of various generations in mobile technology. *28*(7), 328-332.

Han, C. Z.; Xiao, L.; Chen, Z.; Yuan, T. Co-Located Self-Neutralized Handset Antenna Pairs With Complementary Radiation Patterns for 5G MIMO Applications. *IEEE Access*, 2020, 8, 73151-73163.

Hsu, S.-H., Chang, K. J. I. a., & letters, w. p. (2007). A novel reconfigurable microstrip antenna with switchable circular polarization. *6*, 160-162.

Huang, H.-C. (2018). *Overview of antenna designs and considerations in 5G cellular phones.* Paper presented at the 2018 International Workshop on Antenna Technology (iWAT).

Hussain, N., Jeong, M.-J., Abbas, A., & Kim, N. J. I. A. (2020). Metasurface-based single-layer wideband circularly polarized MIMO antenna for 5G millimeter-wave systems. *8*, 130293-130304.

Iqbal, J., Illahi, U., Sulaiman, M. I., Alam, M. M., Su'ud, M. M., & Yasin, M. N. M. J. I. A. (2019). Mutual coupling reduction using hybrid technique in wideband circularly polarized MIMO antenna for WiMAX applications. *7*, 40951-40958.

Irene, G., & Rajesh, A. J. J. o. C. E. (2018). A dual-polarized UWB–MIMO antenna with IEEE 802.11 ac band-notched characteristics using split-ring resonator. *17*(3), 1090-1098.

Jebbawi, K., Egels, M., Pannier, P. J. M., & Letters, O. T. (2020). A novel compact circularly polarized tag antenna with differential-RFIC for EU UHF RFID applications. *62*(4), 1621-1627.

Ji, Z. et al. Low Mutual Coupling Design for 5G MIMO Antennas Using Multi-Feed Technology and Its Application on Metal-Rimmed Mobile Phones. *IEEE Access*, 2021, 9, 151023-151036.

Kabalci, E., & Kabalci, Y. (2019). *Smart grids and their communication systems*: Springer.

Kavas, A., & Kırık, E. (2016). *Antenna design for smart devices.* Paper presented at the 2016 24th Signal Processing and Communication Application Conference (SIU).

Khoshniat, A. (2011). *A linearly and circularly polarized active integrated antenna*: Utah State University.

Kiani, S. H., Altaf, A., Abdullah, M., Muhammad, F., Shoaib, N., Anjum, M. R., . . . Blažauskas, T. J. M. (2020). Eight element side edged framed MIMO antenna array for future 5G smart phones. *11*(11), 956.

Krumbein, A. J. S. A. (2016). Understanding the basics of MIMO communication Technology.

Kumar, P., Urooj, S., & Alrowais, F. J. A. S. (2020). Design and implementation of quad-port MIMO antenna with dual-band elimination characteristics for ultra-wideband applications. *10*(5), 1715.

Kumar, S., Lee, G. H., Kim, D. H., Mohyuddin, W., Choi, H. C., Kim, K. W. J. M., & Letters, O. T. (2020). Multiple-input-multiple-output/diversity antenna with dual band-notched characteristics for ultra-wideband applications. *62*(1), 336-345.

Li, Y., Luo, Y., Yang, G. J. I. T. o. A., & Propagation. (2019). High-isolation 3.5 GHz eight-antenna MIMO array using balanced open-slot antenna element for 5G smartphones. *67*(6), 3820-3830.

Li, S., Fu, B., & Cao, W. (2020). *A miniatured Hexagon-shaped UWB Antenna.* Paper presented at the 2020 IEEE 3rd International Conference on Electronic Information and Communication Technology (ICEICT).

Mathur, R., Dwari, S. J. A.-I. J. o. E., & Communications. (2018). Compact CPW-Fed ultrawideband MIMO antenna using hexagonal ring monopole antenna elements. *93*, 1-6.

Midya, M., Bhattacharjee, S., Mitra, M. J. I. A., & Letters, W. P. (2019). Broadband circularly polarized planar monopole antenna with G-shaped parasitic strip. *18*(4), 581-585.

Molins-Benlliure, J., Cabedo-Fabrés, M., Antonino-Daviu, E., & Ferrando-Bataller, M. J. I. A. (2022). Sector Unit-Cell Methodology for the Design of Sub-6 GHz 5G MIMO Antennas. *10*, 100824-100836.

Narbudowicz, A. Z. J. P. D., Dublin Institute of Technology. (2013). Advanced circularly polarised microstrip patch antennas.

Ofcom. (8 February 2017). 5G spectrum in the UK.

Ojaroudi Parchin, N., Jahanbakhsh Basherlou, H., IA Al-Yasir, Y., M. Abdulkhaleq, A., & A. Abd-Alhameed, R. J. S. (2020). Ultra-wideband diversity MIMO antenna system for future mobile handsets. *20*(8), 2371.

Panahi, A. J. D. t. (2015). Reconfigurable monopole antennas with circular polarization.

Parchin, N. O., Al-Yasir, Y. I. A., Ali, A. H., Elfergani, I., Noras, J. M., Rodriguez, J., & Abd-Alhameed, R. A. J. I. a. (2019). Eight-element dual-polarized MIMO slot antenna system for 5G smartphone applications. *7*, 15612-15622.

Sangodoyin, S., & Molisch, A. F. J. I. T. o. W. c. (2018). Impact of body mass index on ultrawideband MIMO BAN channels—Measurements and statistical model. *17*(9), 6067-6081.

Saxena, S., Kanaujia, B. K., Dwari, S., Kumar, S., Choi, H. C., & Kim, K. W. J. I. A. (2020). Planar four-port dual circularly-polarized MIMO antenna for sub-6 GHz band. *8*, 90779-90791.

Shah, A. S. (2022). A Survey From 1G to 5G Including the Advent of 6G: Architectures, Multiple Access Techniques, and Emerging Technologies. Paper presented at the 2022 IEEE 12th Annual Computing and Communication Workshop and Conference (CCWC).

Shah, A. S. D. (2022). Architecture of Emergency Communication Systems in Disasters through UAVs in 5G and Beyond. 7(1), 25.

Shoaib, N., Shoaib, S., Khattak, R. Y., Shoaib, I., Chen, X., & Perwaiz, A. J. I. A. (2018). MIMO antennas for smart 5G devices. *6*, 77014-77021.

Simone, M., Fanti, A., Lodi, M. B., Pisanu, T., & Mazzarella, G. J. A. S. (2021). An in-line coaxial-to-waveguide transition for Q-band single-feed-per-beam antenna systems. *11*(6), 2524.

Subhanrao Bhadade, R., & Padmakar Mahajan, S. J. E. (2019). Circularly polarized 4× 4 MIMO antenna for WLAN applications. *39*(5), 325-342.

Sun, L.; Li, Y.; Zhang, Z.; Feng, Z. Wideband 5G MIMO Antenna With Integrated Orthogonal-Mode Dual-Antenna Pairs for Metal-Rimmed Smartphones. *IEEE Transactions on Antennas and Propagation*, 2020, 68, 2494-2503.

Talwar, S., Choudhury, D., Dimou, K., Aryafar, E., Bangerter, B., & Stewart, K. (2014). *Enabling technologies and architectures for 5G wireless.* Paper presented at the 2014 IEEE MTT-S International Microwave Symposium (IMS2014).

Tsoulos, G. (2018). *MIMO system technology for wireless communications*: CRC press.

Wallace, J. W., & Jensen, M. A. J. I. t. o. w. c. (2004). Mutual coupling in MIMO wireless systems: A rigorous network theory analysis. *3*(4), 1317-1325.

Wu, C.-H., Chiu, C.-L., Ma, T.-G. J. I. A., & Letters, W. P. (2015). Very compact fully lumped decoupling network for a coupled two-element array. *15*, 158-161.

Wu, Z., Yang, L., Sun, Q. J. J. o. G., & Science, G. (2022). Detection, Estimation and Compensation of Ionospheric Effect on SAR Interferogram Using Azimuth Shift. *5*(1), 14.

Xiong, X., Ling, B. W.-K., Zhang, H., Zhang, G. J. J. o. E. W., & applications. (2018). Coplanar waveguide fed multiple input multiple output antenna with higher isolation and multi-sense circular polarization. *32*(6), 685-694.

Xu, R., Li, J., Qi, Y.-X., Guangwei, Y., Yang, J.-J. J. I. A., & Letters, W. P. (2017). A design of triple-wideband triple-sense circularly polarized square slot antenna. *16*, 1763-1766.

Yassein, M. B., Aljawarneh, S., & Al-Sadi, A. (2017). *Challenges and features of IoT communications in 5G networks.* Paper presented at the 2017 International Conference on Electrical and Computing Technologies and Applications (ICECTA).

Zerihun, B. M., & Wondie, Y. (2017). *Massive MIMO for 5G cellular networks: potential benefits and challenges.* Paper presented at the International Conference on Information and Communication Technology for Develoment for Africa.

Zhang, J., Ge, X., Li, Q., Guizani, M., & Zhang, Y. J. I. W. c. (2016). 5G millimeter-wave antenna array: Design and challenges. *24*(2), 106-112.

Zhang, S., Pedersen, G. F. J. I. a., & letters, w. p. (2015). Mutual coupling reduction for UWB MIMO antennas with a wideband neutralization line. *15*, 166-169.

Paper

1. Dunya Jassim Al-Bu Mohammed, A. F. M. Shahen Shah, Al-Sakib Khan Pathan, and Khaled Rabie, ''Designing An Effective MIMO Antenna for 5G '', submitted to Energies, 2022.